

Machine Unlearning in Low-Dimensional Feature Subspace

Kun Fang ^{*1} Qinghua Tao ^{*2} Junxu Liu ¹ Yixin Xiao ¹ Qingqing Ye ¹ Jian Sun ² Haibo Hu ¹

Abstract

Machine Unlearning (MU) aims at removing the influence of specific data from a pretrained model while preserving performance on the remaining data. In this work, a novel perspective for MU is presented upon low-dimensional feature subspaces, which gives rise to the potentials of separating the remaining and forgetting data herein. This separability motivates our LOFT, a method that proceeds unlearning in a LOw-dimensional FeaTure subspace from the pretrained model skithrough principal projections, which are optimized to maximally capture the information of the remaining data and meanwhile diminish that of the forgetting data. In training, LOFT simply optimizes a small-size projection matrix flexibly plugged into the pretrained model, and only requires one-shot feature fetching from the pretrained backbone instead of repetitively accessing the raw data. Hence, LOFT mitigates two critical issues in mainstream MU methods, i.e., the privacy leakage risk from massive data reload and the inefficiency of updates to the entire pretrained model. Extensive experiments validate the significantly lower computational overhead and superior unlearning performance of LOFT across diverse models, datasets, tasks, and applications. Code is anonymously available at <https://anonymous.4open.science/r/4352/>.

1. Introduction

Deep Neural Networks (DNNs) pretrained on large-scale data, e.g., web-crawled data, greatly advocate various applications (Schuhmann et al., 2022; Zha et al., 2025). However, it also raises significant privacy concerns due to its heavy reliance on massive data. Modern data regulatory frameworks,

^{*}Equal contribution ¹Department of Electrical and Electronic Engineering, The Hong Kong Polytechnic University, Hong Kong, China ²School of Automation, Beijing Institute of Technology, Beijing, China. Correspondence to: Jian Sun <sunjian@bit.edu.cn>, Haibo Hu <haibo.hu@polyu.edu.hk>.

Preprint. February 2, 2026.

such as GDPR (Hoofnagle et al., 2019), emphasizes to preserve *the right to be forgotten* when requesting to delete particular data, e.g., private user data. To address this challenge, Machine Unlearning (MU) (Bourtoule et al., 2021) has emerged and attracted increasing interests in recent years. MU targets on dual goals, i.e., erasing the knowledge from the deleted (forgotten) data and meanwhile preserving the model performance. A gold-standard approach to MU is to retrain the model from scratch based on the remaining data only, i.e., the entire training data excluding the forgetting data (Thudi et al., 2022b), which is called *the exact MU*. Such a retraining process is computationally expensive, especially for modern DNNs which are commonly large-scale models trained on massive data. Hence, a surge of researches on *approximate MU* (Izzo et al., 2021) has been developed to approach the ideal performance of the retrained model.

Existing approximate MU methods generally update the parameters of the original model pretrained on the entire training data \mathcal{D} , so as to align its outputs with that of the ideal model retrained in the exact MU. The core idea here is to proceed the parameter updates with an optimization objective that jointly penalizes the performance on the forgetting data \mathcal{D}_{fg} and maintains that on the remaining data \mathcal{D}_{rm} , with $\mathcal{D}_{fg} \cup \mathcal{D}_{rm} = \mathcal{D}$ and $\mathcal{D}_{fg} \cap \mathcal{D}_{rm} = \emptyset$. This optimization objective leads to different ways to modify the pretrained model, including fine-tuning only on \mathcal{D}_{rm} (Warnecke et al., 2021), assigning random labels to \mathcal{D}_{fg} (Golatkar et al., 2020), conducting gradient ascent on \mathcal{D}_{fg} (Thudi et al., 2022a), masking those parameters sensitive to \mathcal{D}_{fg} (Fan et al., 2024), distilling an additional network (Chundawat et al., 2023a; Zhou et al., 2025), etc. Detailed explanations and discussions on these MU methods are provided in Appendix A. While enabling good performance, we note their two critical drawbacks far underexplored:

- **Frequent revisits to the massive training data.** Existing MU methods generally request to visit training samples in both \mathcal{D}_{rm} and \mathcal{D}_{fg} during the iterative parameter updates to the pretrained model. Such massive data fetching not only incurs expensive computational overhead, but also poses privacy threats during the frequent access to (user) data.
- **Iterative modifications to the pretrained model.** Whenever a particular dataset \mathcal{D}_{fg} is requested to be forgotten, parameters of the pretrained model have to be updated, yield-

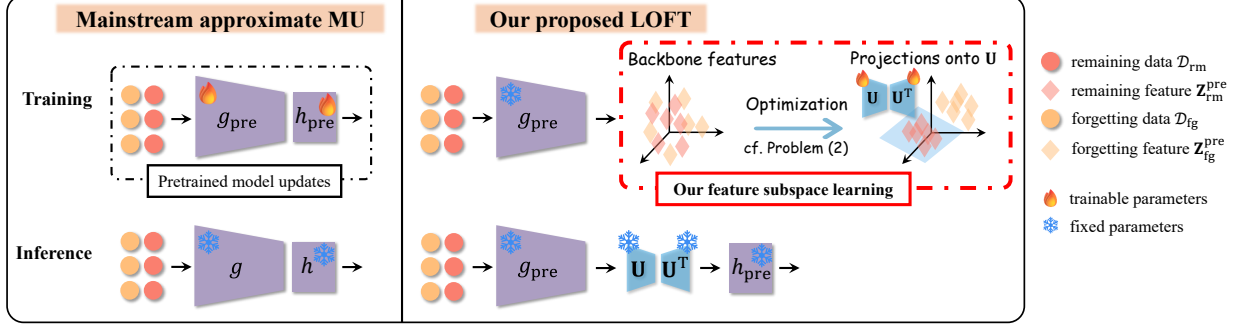


Figure 1. Overview of our proposed LOFT and mainstream approximate MU methods. After unlearning, the trained projection matrix of LOFT is incorporated into the model’s forward propagation during inference, with details in Sec.4.2.

ing a new model tailored to \mathcal{D}_{fg} . This can be computationally infeasible in practice, as each unlearning request demands a new model modified from the pretrained one.

In this work, we aim to address the above challenges in approximate MU methods. (i) Firstly, a new perspective to study MU in *low-dimensional feature subspaces* is introduced. We reveal the potential separability in feature subspaces between \mathcal{D}_{fg} and \mathcal{D}_{rm} on the retrained model when comparing to the pretrained model. (ii) Then, the observed separability inspires us to *learn a feature subspace* from the pretrained model to achieve unlearning. To this end, the feature subspace is optimized to differentiate \mathcal{D}_{fg} and \mathcal{D}_{rm} by capturing maximal information of the features w.r.t. \mathcal{D}_{rm} and meanwhile describing minimal information w.r.t. \mathcal{D}_{fg} . This optimization is implemented following the spirits of Principal Component Analysis (PCA) (Pearson, 1901): A projection matrix is trained and inserted into the pretrained model, requiring only two feature covariance matrices of \mathcal{D}_{fg} and \mathcal{D}_{rm} . Consequently, the knowledge of \mathcal{D}_{fg} can be therein effectively diminished, while that of \mathcal{D}_{rm} gets well preserved in this feature subspace, thus fulfilling the objective of unlearning. Our unlearning method is thereby named LOFT for learning LOw-dimensional FeaTures.

Fig.1 provides an overview of our LOFT and the related mainstream approximate MU methods. LOFT offers efficiency for computation and storage, flexibility in practice, and privacy protection for user data, towards closing the gaps in adapting to real-world MU scenarios:

• **One-shot feature fetching.** LOFT conducts MU in the feature space, and thus only needs to fetch the features outputted from the pretrained model, instead of directly and iteratively accessing training samples, e.g., private user data. Note that once the features are fetched, calculations to the covariance matrix are one-shot, since our PCA-based optimization does not vary the covariance matrix, but only updates projection directions for learning the feature subspace that well distinguishes the knowledge between \mathcal{D}_{rm} and \mathcal{D}_{fg} . Hence, LOFT successfully avoids direct and massive visits

to the training data (user data) for privacy protection and computational efficiency.

• **Plug-in module implementation.** With the spirits from PCA, we design a novel objective to optimize a projection matrix applied to the feature covariances, such that in the projected subspace the features w.r.t. \mathcal{D}_{rm} can be well reconstructed while the features w.r.t. \mathcal{D}_{fg} cannot. This algorithm enables the implementation in a plug-and-play manner: a projection matrix is inserted into the pretrained model, without retraining or fine-tuning the pretrained parameters. This merit is significant for efficiency and real-world practicality. For instance, when handling multiple unlearning requests from different users, LOFT only requires a separate projection module in a rather small size for each request, instead of a new model modified from the pretrained DNN.

The key contributions of this work are summarized below:

- We presents a novel perspective, *feature subspace*, for MU, which to the best of our knowledge is the first time revealing the potential separability between the forgetting and remaining data in low-dimensional feature subspaces.
- A new MU method named LOFT is proposed by leveraging PCA-based subspace learning, simply doing *one-shot feature fetching* and *updating a projection matrix* as a plugged-in module into the pretrained model. LOFT well addresses the aforementioned crucial issues of massive data access and pretrained model modification in MU.
- The objective in LOFT involves two covariance matrices with size depending on the feature dimension and only optimizes a projection matrix, *reducing the parameter number and computing time by orders of magnitude* than mainstream MU methods, as demonstrated in our experiments.
- Extensive experiments verify our superior unlearning accuracy and efficiency on varied datasets, networks, unlearning tasks, and real-world applications.

2. Preliminaries

Machine unlearning. MU aims at maintaining prediction performances of a well-trained model f_{pre} when removing

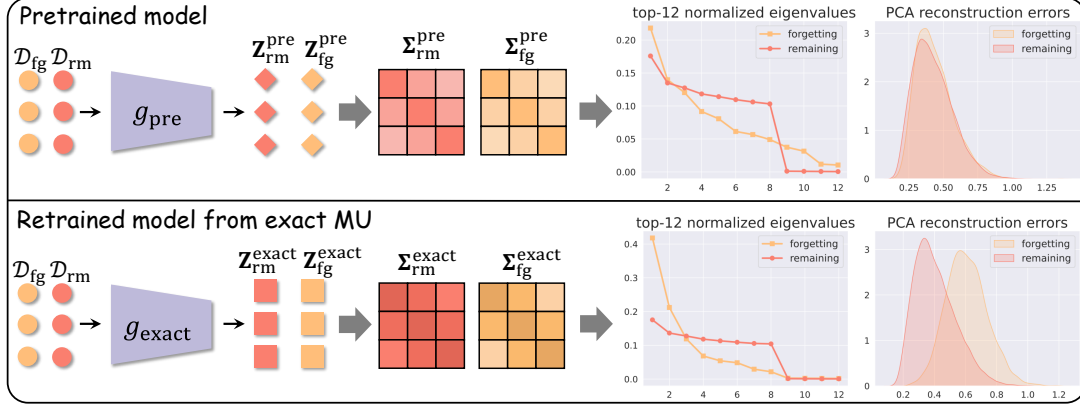


Figure 2. Spectrum and reconstruction analyses on features of \mathcal{D}_{fg} and \mathcal{D}_{rm} w.r.t. the pretrained f_{pre} and the retrained f_{exact} , with results on the top-12 normalized eigenvalues and reconstruction errors.

(or forgetting) specific data (Bouroule et al., 2021). In MU, the model f_{pre} pretrained on the full dataset \mathcal{D} is given. A particular subset \mathcal{D}_{fg} is requested to be forgotten, and we have the remaining data denoted as $\mathcal{D}_{rm} := \mathcal{D} \setminus \mathcal{D}_{fg}$. MU seeks to erase the knowledge of \mathcal{D}_{fg} from f_{pre} and meanwhile to preserve the performance on \mathcal{D}_{rm} . The golden standard in MU is to attain a model f_{exact} retrained from scratch on \mathcal{D}_{rm} , i.e., the exact MU (Thudi et al., 2022b). In contrast, fine-tuning the pretrained model f_{pre} to approximate the ideal performances of f_{exact} has been a central research focus for flexibility and efficiency, namely the approximate MU (Izzo et al., 2021). We provide more discussions on related work in Appendix A.

Principal component analysis. PCA has long been a fundamental tool in machine learning and beyond (Pearson, 1901). PCA seeks orthogonal directions, i.e., principal components capturing the highest projection variance, so as to keep maximal data information. These directions can be obtained by taking the eigenvectors of the input covariance matrix. PCA can explore the intrinsic patterns residing in low-dimension subspaces spanned by those principal components, and has been studied for learning with modern DNNs, e.g., training algorithms (Li et al., 2023b) and anomaly detection applications (Fang et al., 2024). In this work, we follow the spirits of PCA for MU by *learning* the projection directions associated with the low-dimensional feature subspace from f_{pre} .

Notations. Let $f_{pre} : \mathcal{X} \rightarrow \mathbb{R}^C$ be a DNN pretrained on $\mathcal{D} = \{\mathbf{x}_i, y_i\}_{i=1}^N \subseteq \mathcal{X} \times \mathcal{Y}$, with samples $\mathbf{x}_i \in \mathcal{X} \subset \mathbb{R}^D$ and their labels $y_i \in \mathcal{Y} = \{1, 2, \dots, C\}$. The model $f(\cdot)$ takes \mathbf{x} as the input and outputs C -dimensional logits $f(\mathbf{x}) \in \mathbb{R}^C$ for classification prediction. More specifically, f can be structured with a backbone $g : \mathcal{X} \rightarrow \mathbb{R}^d$ and a linear layer $h : \mathbb{R}^d \rightarrow \mathbb{R}^C$ in sequence, where $g(\cdot)$ learns the (penultimate-layer) feature $\mathbf{z} = g(\mathbf{x}) \in \mathbb{R}^d$ and then the

linear layer $h(\cdot)$ is applied to the feature \mathbf{z} for the output logits, i.e., $f(\mathbf{x}) = h(g(\mathbf{x}))$.

3. Feature Subspace Perspective for Approximate MU

In this section, we introduce the perspective of feature subspaces to decouple the impacts of the forgetting data \mathcal{D}_{fg} from the remaining data \mathcal{D}_{rm} in approximate MU. This feature-based perspective helps explore the intrinsic differences between the pretrained f_{pre} and the retrained f_{exact} in low-dimensional subspaces of their learned features, advocating efficient MU with private data protection.

The pretrained f_{pre} is learned with the entire training dataset $\mathcal{D} = \mathcal{D}_{fg} \cup \mathcal{D}_{rm}$. In contrast, the ideal model f_{exact} from the exact MU is trained exclusively on \mathcal{D}_{rm} and never sees \mathcal{D}_{fg} . This fundamental distinction in their training paradigms motivates our exploration on the learned features \mathbf{z} w.r.t. \mathcal{D}_{fg} and \mathcal{D}_{rm} from f_{pre} and f_{exact} , respectively. To be specific, we consider the potential separability between \mathcal{D}_{fg} and \mathcal{D}_{rm} through feature-based perspectives, naturally assuming that the unseen forgetting data \mathcal{D}_{fg} are easy to be differentiated from the seen \mathcal{D}_{rm} in the feature space learned in the exact MU model f_{exact} . We in accordance make the following hypothesis:

(H) For the exact MU model f_{exact} , there exists a low-dimensional feature subspace, where the features of \mathcal{D}_{fg} and \mathcal{D}_{rm} are easy to be separated, while for the pretrained model f_{pre} , the features of \mathcal{D}_{fg} and \mathcal{D}_{rm} remain distinctively less separable.

In the following, both empirical evidences and theoretical analysis are provided to support **(H)**. Particularly, PCA is applied to features $\mathbf{z} \in \mathbb{R}^d$ from the network backbone, in order to explore the intrinsic structures. We denote the features of the forgetting data \mathcal{D}_{fg} and the remaining data \mathcal{D}_{rm}

from g_{pre} and g_{exact} as $\mathbf{Z}_{\text{fg}}^{\text{pre}}, \mathbf{Z}_{\text{rm}}^{\text{pre}}, \mathbf{Z}_{\text{fg}}^{\text{exact}}, \mathbf{Z}_{\text{rm}}^{\text{exact}}$ and their covariance matrices as $\Sigma_{\text{fg}}^{\text{pre}}, \Sigma_{\text{rm}}^{\text{pre}}, \Sigma_{\text{fg}}^{\text{exact}}, \Sigma_{\text{rm}}^{\text{exact}} \in \mathbb{R}^{d \times d}$, respectively. With eigen-decomposition to those covariance matrices, we investigate their eigenvalues and reconstruction performances, which is illustrated in Fig.2.

Spectrum analysis. Fig.2 visualizes the eigen-decay (i.e., the distribution of variance across principal components) for the aforementioned covariance matrices. In the pretrained f_{pre} , the decays in eigenvalues of $\Sigma_{\text{fg}}^{\text{pre}}$ and $\Sigma_{\text{rm}}^{\text{pre}}$ exhibit similar trends. In contrast, a marked divergence appears in the retrained f_{exact} : $\Sigma_{\text{fg}}^{\text{exact}}$ shows a distinctly sharper eigenvalue decay than $\Sigma_{\text{rm}}^{\text{exact}}$. This sharper decay indicates that, after exact unlearning, features of \mathcal{D}_{fg} becomes concentrated in fewer dominant directions, while \mathcal{D}_{rm} retains a more dispersed structure. This spectrum divergence reveals the potential of achieving unlearning within the feature subspace, rather than typically approaching the outputs or parameters of f_{exact} in existing approximate MU methods.

Reconstruction analysis. The PCA reconstruction error quantitatively measures the captured information along projection directions. We apply PCA to the remaining features \mathbf{Z}_{rm} and obtain $\mathbf{U}_{\text{rm}} \in \mathbb{R}^{d \times s}$ projecting features onto the s -dimensional subspace. The reconstruction error for a centered feature \bar{z} is calculated as $e = \|\mathbf{U}_{\text{rm}} \mathbf{U}_{\text{rm}}^{\top} \bar{z} - \bar{z}\|_2$. In Fig.2, we compute such errors on both \mathbf{Z}_{rm} and \mathbf{Z}_{fg} of f_{pre} and f_{exact} , respectively. The reconstruction errors for $\mathbf{Z}_{\text{fg}}^{\text{pre}}$ and $\mathbf{Z}_{\text{rm}}^{\text{pre}}$ of the pretrained f_{pre} are very similar, while those for $\mathbf{Z}_{\text{fg}}^{\text{exact}}$ and $\mathbf{Z}_{\text{rm}}^{\text{exact}}$ of the retrained f_{exact} appear distinctively different. The results suggest that the subspace learned from $\mathbf{Z}_{\text{rm}}^{\text{exact}}$ fails to capture the intrinsic patterns of $\mathbf{Z}_{\text{fg}}^{\text{exact}}$, making them easily separable therein and thus supporting the aforementioned hypothesis (**H**).

Analytical evidence. We provide theoretical evidence on reconstruction analyses for the hypothesis (**H**), supporting the promising perspective of learning a low-dimensional feature subspace that can separate \mathcal{D}_{fg} and \mathcal{D}_{rm} under the exact MU model f_{exact} . This result is stated in the following Lemma 3.1 with proof in Appendix B.

Lemma 3.1. *Given the feature covariance $\Sigma_{\text{rm}}^{\text{exact}}$ from f_{exact} on \mathcal{D}_{rm} , its eigendecomposition is given by $\Sigma_{\text{rm}}^{\text{exact}} = \mathbf{V} \Lambda \mathbf{V}^{\top}$ with eigenvalues $\lambda_1 \geq \lambda_2 \geq \dots \geq \lambda_n$. There exists an s -dimensional subspace $\text{range}(\mathbf{U}_*)$ spanned by the top- s principal directions of $\Sigma_{\text{rm}}^{\text{exact}}$ ($\mathbf{U}_* = \mathbf{V}_{:,1:s}$), such that for any $\mathbf{x} \in \mathcal{D}_{\text{rm}}$, its features can be well reconstructed by the subspace $\text{range}(\mathbf{U}_*)$, while for any $\mathbf{x} \in \mathcal{D}_{\text{fg}}$, its features hold minor projected information in $\text{range}(\mathbf{U}_*)$. Mathematically, we have small positive numbers $\epsilon_{\text{rm}}, \epsilon_{\text{fg}} > 0$ that satisfies*

$$\begin{aligned} \|(\mathbf{I} - \mathbf{U}_* \mathbf{U}_*^{\top}) g_{\text{exact}}(\mathbf{x})\|_2 &\leq \epsilon_{\text{rm}}, \quad \forall \mathbf{x} \in \mathcal{D}_{\text{rm}}, \\ \|\mathbf{U}_* \mathbf{U}_*^{\top} g_{\text{exact}}(\mathbf{x})\|_2 &\leq \epsilon_{\text{fg}}, \quad \forall \mathbf{x} \in \mathcal{D}_{\text{fg}}. \end{aligned} \quad (1)$$

This insight unveils the distinction between features \mathbf{Z}_{rm} and \mathbf{Z}_{fg} in low-dimensional subspaces w.r.t. f_{exact} and can advocate novel unlearning methodologies from the raised new perspective, such as our LOFT introduced in Sec.4.

4. Approximate MU with Subspace Learning

Grounded on the feature subspace perspective and the analysis in Sec.3, we now focus on how to attain a preferable feature subspace for f_{pre} , such that the features $\mathbf{Z}_{\text{rm}}^{\text{pre}}$ and $\mathbf{Z}_{\text{fg}}^{\text{pre}}$ can be well distinguished in this subspace, i.e., diminishing the knowledge of \mathcal{D}_{fg} and preserving that of \mathcal{D}_{rm} from f_{pre} . Accordingly, we name this proposed method as LOFT, learning LOw-dimensional FeaTure subspaces. Apart from approaching the outputs or parameters of the exact retrained f_{exact} , LOFT leads to an interesting and promising direction of formulating unlearning models that pertain similar properties in feature (sub)spaces, which we hope could bring new perspectives and opportunities in MU.

4.1. Optimization

LOFT aims to find an s -dimensional subspace $\text{range}(\mathbf{U})$ for the d -dimensional features of the pretrained model f_{pre} . This linear subspace is in fact given by the span of the orthonormal columns of the $d \times s$ matrix $\mathbf{U} = [\mathbf{u}_1, \dots, \mathbf{u}_s]$, the set of which defines the well-known Stiefel manifold $\text{St}(d, s)$ with $d \geq s$. Towards the feature separability for unlearning, LOFT follows the spirits from PCA to seek such a subspace (to optimize \mathbf{U}), in which the information of $\mathbf{Z}_{\text{rm}}^{\text{pre}}$ is maximally captured and meanwhile that of the forgetting features $\mathbf{Z}_{\text{fg}}^{\text{pre}}$ gets minimally described.

Proposition 4.1. *Let \mathbf{M} be an $l \times l$ symmetric matrix. Let $\gamma_1, \dots, \gamma_m$ be its m smallest eigenvalues, possibly including multiplicities, with associated orthonormal eigenvectors $\mathbf{v}_1, \dots, \mathbf{v}_m$. Let \mathbf{V} be a matrix whose columns are these eigenvectors. Then, the optimization problem $\min_{\mathbf{U} \in \text{St}(l, m)} \text{Tr}(\mathbf{U}^{\top} \mathbf{M} \mathbf{U})$ has a minimizer at $\mathbf{U}_* = \mathbf{V}$ and we have $\mathbf{U}_*^{\top} \mathbf{M} \mathbf{U}_* = \text{diag}(\boldsymbol{\Gamma})$ with $\boldsymbol{\Gamma} = [\gamma_1, \dots, \gamma_m]^{\top}$, where $\text{Tr}(\cdot)$ denotes the matrix trace.*

Proposition 4.1 (Panay et al., 2022) formalizes the optimization problem for obtaining the projection directions capturing minimal information in PCA with Stiefel manifold, where \mathbf{M} denotes the covariance matrix. This correspondingly leads to the optimization problem for the projection directions capturing maximal information: the subspace spanned by the eigenvectors of \mathbf{M} with the m largest eigenvalues is obtained by solving $\min_{\mathbf{U} \in \text{St}(l, m)} \text{Tr}(\mathbf{M} - \mathbf{U} \mathbf{U}^{\top} \mathbf{M} \mathbf{U} \mathbf{U}^{\top})$, which also corresponds to the reconstruction error of PCA as similarly explained in Sec 4.1 of (Avron et al., 2014). In LOFT, we establish the following objective

to learn the subspace, specifically for the purpose of MU:

$$\min_{\mathbf{U} \in \text{St}(d, s)} J(\mathbf{U}) = \underbrace{\left(\frac{\text{Tr}(\mathbf{U}^\top \Sigma_{\text{fg}}^{\text{pre}} \mathbf{U})}{\text{Tr}(\Sigma_{\text{fg}}^{\text{pre}})} \right)^2}_{J_{\text{fg}}} + \underbrace{\left(\frac{\text{Tr}(\Sigma_{\text{rm}}^{\text{pre}} - \mathbf{U} \mathbf{U}^\top \Sigma_{\text{rm}}^{\text{pre}} \mathbf{U} \mathbf{U}^\top)}{\text{Tr}(\Sigma_{\text{rm}}^{\text{pre}})} \right)^2}_{J_{\text{rm}}}, \quad (2)$$

where the numerators play key roles and the denominators balance normalization. The patterns of \mathcal{D}_{rm} get preserved with J_{rm} , while that of \mathcal{D}_{fg} gets diminished with J_{fg} . The joint optimization of J_{rm} and J_{fg} advocates the separability between $\mathbf{Z}_{\text{rm}}^{\text{pre}}$ and $\mathbf{Z}_{\text{fg}}^{\text{pre}}$ in the subspace projected via \mathbf{U} :

- J_{fg} quantifies the projection variance of the forgetting features $\mathbf{Z}_{\text{fg}}^{\text{pre}}$ onto the subspace spanned by \mathbf{U} , as explained in Proposition 4.1. Minimizing J_{fg} encourages \mathbf{U} to capture minimal information of $\mathbf{Z}_{\text{fg}}^{\text{pre}}$, aiming to forget the knowledge of \mathcal{D}_{fg} .
- J_{rm} measures the projection variance of the remaining features $\mathbf{Z}_{\text{rm}}^{\text{pre}}$ captured within the complement subspace w.r.t. \mathbf{U} , namely the reconstruction error. Minimizing J_{rm} forces \mathbf{U} to preserve maximal information of $\mathbf{Z}_{\text{rm}}^{\text{pre}}$, so as to maintain model performance on \mathcal{D}_{rm} .

4.2. Implementation and Discussion

LOFT simply requires to optimize the projection matrix \mathbf{U} applied to features $\mathbf{Z}_{\text{fg}}^{\text{pre}}$ and $\mathbf{Z}_{\text{rm}}^{\text{pre}}$ from the pretrained f_{pre} . In implementation, a projection module associated with parameters \mathbf{U} is inserted primarily between the backbone g_{pre} and the last linear layer h_{pre} , so as to encode penultimate-layer features into a subspace $\text{range}(\mathbf{U})$ via an orthogonal projector $\mathbf{U} \mathbf{U}^\top$. During training, the Riemannian optimizer (Becigneul & Ganea, 2019; Kochurov et al., 2020) is deployed for $J(\mathbf{U})$ with \mathbf{U} optimized on the Stiefel manifold $\text{St}(d, s)$. During inference, the resulting model from LOFT for unlearning is given by $f_{\mathbf{U}}(\cdot) \triangleq h_{\text{pre}}(\mathbf{U} \mathbf{U}^\top g_{\text{pre}}(\cdot))$, in contrast to the original pretrained model $f_{\text{pre}} = h_{\text{pre}}(g_{\text{pre}}(\cdot))$, as demonstrated in Fig.1.

One-shot feature fetching. The computation to $J(\mathbf{U})$ relies on the two covariance matrices $\Sigma_{\text{rm}}^{\text{pre}}$ and $\Sigma_{\text{fg}}^{\text{pre}}$ w.r.t. features from f_{pre} . Once $\Sigma_{\text{rm}}^{\text{pre}}$, $\Sigma_{\text{fg}}^{\text{pre}}$ are computed, LOFT proceeds to optimize the $d \times s$ projection matrix \mathbf{U} and thus only conducts one-shot feature fetching. This differs fundamentally from existing approximate MU methods, which must repeatedly access the original training data at each optimization iteration. By eliminating the need for such direct and massive visits to data samples, LOFT significantly reduces computational overhead and inherently strengthens privacy protection on (user) data in real-world MU.

Plug-in module implementation. Compared to fine-tuning or retraining all parameters in f_{pre} , LOFT optimizes a $d \times s$ matrix as in (2), the parameter number of which is thereby reduced by orders of magnitude. Thus, LOFT takes significantly less computation overhead than the exact MU and mainstream approximate MU methods, supported by numerical results in Sec.5.2. In implementation, LOFT flexibly serves as a plug-in module into the pretrained model f_{pre} , without modifying parameters of f_{pre} . This merit is of great practicality in real-world deployment: in cases of handling multiple unlearning requests from different users, each request can be addressed by efficiently optimizing a small-size projection matrix, instead of maintaining multiple models refined from f_{pre} .

Theoretical guarantee. LOFT offers a novel feature subspace perspective and an empirical method for MU. We position LOFT as orthogonal and complementary to the established research on certified unlearning (Guo et al., 2020). Certified methods provide rigorous guarantees via differential privacy (Dwork, 2006) by bounding the parameter difference between approximate and exact unlearned models. In contrast, LOFT operates on a fundamentally different principle. Instead of updating parameters of f_{pre} , LOFT applies a learnable projection matrix \mathbf{U} on features from f_{pre} to achieve unlearning in a feature subspace sense. This fundamental difference implies that existing theoretical framework designed for certifying parameter proximity are not directly applicable to LOFT. Nevertheless, we seek theoretical guarantees for LOFT and shed light on the output difference between our $f_{\mathbf{U}}$ and the retrained f_{exact} , as formalized in Theorem 4.2 with proofs in Appendix B. This analysis provides fundamental theoretical support for LOFT, while a more rigorous theoretical development remains a valuable direction for future work.

Theorem 4.2. Suppose that $J(\mathbf{U})$ is optimized with a stationary point $\hat{\mathbf{U}}$ that approximates the optimal solution \mathbf{U}_* with a small gap $\epsilon_{\text{opt}} > 0$, such that $\|\mathbf{U}_* \mathbf{U}_*^\top - \hat{\mathbf{U}} \hat{\mathbf{U}}^\top\|_F \leq \epsilon_{\text{opt}}$, then, for any $\mathbf{x} \in \mathcal{D}$, the difference of outputs between the unlearned model $f_{\hat{\mathbf{U}}}$ and the exact MU model f_{exact} is bounded by a constant C : $\|f_{\hat{\mathbf{U}}}(\mathbf{x}) - f_{\text{exact}}(\mathbf{x})\|_2 \leq C$ with C dependent on ϵ_{opt} .

5. Experiments

In this section, extensive experiments are conducted to evaluate LOFT, showing its potentials of low-dimensional feature subspace perspective for MU. In experiments, we primarily focus on the *class-centric* unlearning (Zhou et al., 2025), widely studied in real-world scenarios, as data from different users can represent varied classes, where setups of *extreme* and *continual* unlearning are further explored in Appendix D. The *instance-wise* unlearning is also investigated, which is another significant unlearning type. More

Table 1. Comparison results of Swin-T on Tiny-ImageNet. The ✓ and ✗ indicate whether \mathcal{D}_{rm} and \mathcal{D}_{fg} are involved in optimization. Avg.G. is average accuracy and MIA gap to the retrained model.

method	\mathcal{D}_{rm}	\mathcal{D}_{fg}	$\text{Acc}_{\text{rm}}^{\text{tr}}$	$\text{Acc}_{\text{fg}}^{\text{tr}}$	$\text{Acc}_{\text{rm}}^{\text{te}}$	$\text{Acc}_{\text{fg}}^{\text{te}}$	MIA	Avg.G.↓
pretrained	✓	✓	99.63 \pm 0.01	99.75 \pm 0.20	74.54 \pm 0.16	74.83 \pm 8.14	96.63 \pm 1.02	-
retrained	✓	✗	99.67 \pm 0.03 (0.00)	0.00 \pm 0.00 (0.00)	75.44 \pm 0.19 (0.00)	0.00 \pm 0.00 (0.00)	0.00 \pm 0.00 (0.00)	0.00
GA	✗	✓	88.40 \pm 5.51 (11.27)	23.12 \pm 12.14 (23.12)	65.27 \pm 3.56 (10.17)	18.82 \pm 7.52 (18.82)	19.95 \pm 10.24 (19.95)	16.67
FT	✓	✗	99.92 \pm 0.00 (0.25)	18.73 \pm 5.90 (18.73)	74.25 \pm 0.21 (1.19)	16.17 \pm 6.33 (16.17)	3.73 \pm 2.22 (3.73)	8.02
RL	✗	✓	92.94 \pm 1.91 (6.73)	9.98 \pm 7.44 (9.98)	67.17 \pm 1.46 (8.17)	7.50 \pm 7.57 (7.50)	1.83 \pm 0.54 (1.83)	6.85
RL	✓	✓	99.91 \pm 0.01 (0.24)	1.52 \pm 1.17 (1.52)	74.43 \pm 0.18 (1.01)	0.33 \pm 0.58 (0.33)	0.00 \pm 0.00 (0.00)	0.62
SalUn	✗	✓	93.16 \pm 1.90 (6.51)	13.55 \pm 10.30 (13.55)	67.49 \pm 1.56 (7.95)	10.00 \pm 9.26 (10.00)	3.45 \pm 0.87 (3.45)	8.29
SalUn	✓	✓	99.88 \pm 0.01 (0.21)	2.57 \pm 1.09 (2.57)	74.71 \pm 0.19 (0.73)	1.00 \pm 0.87 (1.00)	0.00 \pm 0.00 (0.00)	0.90
BT	✗	✓	91.70 \pm 1.89 (7.97)	7.72 \pm 5.45 (7.72)	66.35 \pm 1.37 (9.09)	5.50 \pm 6.14 (5.50)	1.40 \pm 0.44 (1.40)	6.34
L2UL	✗	✓	92.69 \pm 3.43 (6.98)	4.43 \pm 0.15 (4.43)	67.69 \pm 2.58 (7.75)	2.00 \pm 0.87 (2.00)	2.57 \pm 0.92 (2.57)	4.75
COUN+RL	✗	✓	92.56 \pm 0.75 (7.11)	10.07 \pm 3.85 (10.07)	67.85 \pm 0.51 (7.59)	5.67 \pm 2.57 (5.67)	2.28 \pm 0.46 (2.28)	6.54
DELETE	✗	✓	99.13 \pm 0.12 (0.54)	13.32 \pm 4.17 (13.32)	73.31 \pm 0.28 (2.13)	6.50 \pm 2.18 (6.50)	1.85 \pm 0.48 (1.85)	4.88
LOFT	only $\Sigma_{\text{rm}}^{\text{pre}}$	only $\Sigma_{\text{fg}}^{\text{pre}}$	98.59 \pm 0.07 (1.08)	1.48 \pm 1.27 (1.48)	74.27 \pm 0.18 (1.17)	0.50 \pm 0.50 (0.50)	0.00 \pm 0.00 (0.00)	0.85

Table 2. Comparison on computational costs w.r.t. the results in Table 1. The detailed counts and percentages of optimized parameters are listed. RTE is the run time efficiency in seconds on single NVIDIA GeForce RTX 4090 GPU. For LOFT, RTE measures only the optimization time of (2), as training features can be pre-calculated in practice and covariances are readily available for on-demand use.

method	\mathcal{D}_{rm}	\mathcal{D}_{fg}	# optimized param. (%)	RTE (seconds) ↓	additional requirements
pretrained	✓	✓	27,673,154 (100%)	882.05	-
retrain	✓	✗	27,673,154 (100%)	858.14	-
FT	✓	✗	27,673,154 (100%)	428.24	-
GA	✗	✓	27,673,154 (100%)	13.49	-
RL	✗	✓	27,673,154 (100%)	13.19	-
RL	✓	✓	27,673,154 (100%)	438.48	-
SalUn	✗	✓	13,836,577 (50%)	15.00	a parameter saliency mask
SalUn	✓	✓	13,836,577 (50%)	450.23	a parameter saliency mask
BT	✗	✓	27,673,154 (100%)	14.32	a randomly-initialized teacher model
L2UL	✗	✓	27,673,154 (100%)	15225.05	a set of adversarial examples; a parameter importance mask
COUN+RL	✗	✓	27,673,154 (100%)	23.45	-
DELETE	✗	✓	27,673,154 (100%)	22.14	a copy of the pretrained model
LOFT	only $\Sigma_{\text{rm}}^{\text{pre}}$	only $\Sigma_{\text{fg}}^{\text{pre}}$	192,000 (0.69%)	0.56	a projection matrix $\mathbf{U} \in \text{St}(768, 250)$

empirical results and discussions on real-world applications and generation tasks are provided in Appendices E and F.

5.1. Setups

Datasets and models. Experiments are executed on Tiny-ImageNet (Le & Yang, 2015) (200 classes, $64 \times 64 \times 3$) and ImageNet-1K (Deng et al., 2009) (1,000 classes, $224 \times 224 \times 3$). We skip comparisons on other easier datasets with smaller scales and distinctively fewer classes, e.g., CIFAR (Krizhevsky, 2009) and SVHN (Netzer et al., 2011), which have been extensively evaluated and yet show almost incremental improvements with limited challenges for class-centric unlearning. Swin-T (Liu et al., 2021) and ResNet50 (He et al., 2016) are evaluated on Tiny-ImageNet and ImageNet-1K, respectively.

Baselines. We compare LOFT with a series of strong baselines: Fine-Tuning (FT) (Warnecke et al., 2021), Gradient Ascent (GA) (Thudi et al., 2022a), Random Labeling (RL) (Golatkar et al., 2020), Salun (Fan et al., 2024), Bad Teaching (BT) (Chundawat et al., 2023a), Learn to UnLearn

(L2UL) (Cha et al., 2024), COUN (Khalil et al., 2025) and DELETE (Zhou et al., 2025). Results of the pretrained f_{pre} and the retrained f_{exact} are also included. See Appendices A and C for baseline outlines and implementation details.

Restricted data access. We underscore the significance of restricted data access for MU. If both \mathcal{D}_{fg} and \mathcal{D}_{rm} are available, even the naive RL method can nearly approach the ideal performance of f_{exact} , as shown in our Table 1. Recent studies have focused on using only \mathcal{D}_{fg} for practicality in real-world setups (Cha et al., 2024; Zhou et al., 2025), while our LOFT advances this direction through a distinctively novel way of optimizing on two feature covariance matrices w.r.t. \mathcal{D}_{fg} and \mathcal{D}_{rm} , without accessing raw data. Accordingly, our comparisons are presented among baselines operating on \mathcal{D}_{fg} . For completeness, methods involving \mathcal{D}_{rm} are included as reference (marked in gray).

Metrics. Four metrics on learning accuracy are leveraged (Zhou et al., 2025): $\text{Acc}_{\text{fg}}^{\text{tr}}$ on the forgetting \mathcal{D}_{fg} and $\text{Acc}_{\text{rm}}^{\text{tr}}$ on the remaining \mathcal{D}_{rm} of the training data, $\text{Acc}_{\text{fg}}^{\text{te}}$ on the

Table 3. Comparison results under single-class unlearning with ResNet50 on ImageNet-1K.

method	\mathcal{D}_{rm}	\mathcal{D}_{fg}	$\text{Acc}_{\text{rm}}^{\text{tr}}$	$\text{Acc}_{\text{fg}}^{\text{tr}}$	$\text{Acc}_{\text{rm}}^{\text{te}}$	$\text{Acc}_{\text{fg}}^{\text{te}}$	Avg.G. \downarrow	RTE \downarrow	# param. (%)
pretrained	✓	✓	77.92 ± 0.01	83.46 ± 7.64	76.15 ± 0.01	81.33 ± 10.26	-	-	25,557,032 (100%)
retrained	✓	✗	80.25 ± 0.16 (0.00)	0.00 ± 0.00 (0.00)	75.72 ± 0.04 (0.00)	0.00 ± 0.00 (0.00)	0.00	-	25,557,032 (100%)
GA	✗	✓	71.87 ± 1.80 (8.38)	0.00 ± 0.00 (0.00)	71.42 ± 1.89 (4.30)	0.00 ± 0.00 (0.00)	3.17	9.32	25,557,032 (100%)
RL	✗	✓	72.11 ± 1.42 (8.14)	1.87 ± 0.69 (1.87)	71.53 ± 1.44 (4.19)	5.33 ± 4.16 (5.33)	4.88	14.40	25,557,032 (100%)
SalUn	✗	✓	71.56 ± 0.68 (8.69)	2.67 ± 0.77 (2.67)	70.84 ± 0.60 (4.88)	4.67 ± 3.06 (4.67)	5.23	27.73	12,778,516 (50%)
BT	✗	✓	72.07 ± 1.53 (8.18)	1.87 ± 0.93 (1.87)	71.49 ± 1.49 (4.23)	5.33 ± 4.16 (5.33)	4.90	16.84	25,557,032 (100%)
COUN+RL	✗	✓	70.04 ± 2.01 (10.21)	1.36 ± 0.35 (1.36)	69.72 ± 1.82 (6.00)	4.67 ± 3.06 (4.67)	5.56	15.24	25,557,032 (100%)
DELETE	✗	✓	72.46 ± 1.30 (7.79)	0.95 ± 0.78 (0.95)	71.90 ± 1.23 (3.82)	2.00 ± 3.46 (2.00)	3.64	17.82	25,557,032 (100%)
LOFT	only $\Sigma_{\text{rm}}^{\text{pre}}$	only $\Sigma_{\text{fg}}^{\text{pre}}$	79.96 ± 0.38 (0.29)	0.00 ± 0.00 (0.00)	69.40 ± 0.35 (6.32)	0.00 ± 0.00 (0.00)	1.65	0.94	1,024,000 (4.01%)

Table 4. Comparison results under instance unlearning with Swin-T on Tiny-ImageNet.

method	\mathcal{D}_{rm}	\mathcal{D}_{fg}	$\text{Acc}_{\text{rm}}^{\text{tr}}$	$\text{Acc}_{\text{fg}}^{\text{tr}}$	Acc_{te}	MIA	Avg.G. \downarrow	RTE \downarrow	# param. (%)
pretrained	✓	✓	99.63 ± 0.00	99.80 ± 0.01	74.55 ± 0.00	96.20 ± 0.44	-	882.05	27,673,154 (100%)
retrained	✓	✗	99.67 ± 0.02 (0.00)	75.97 ± 1.00 (0.00)	75.03 ± 0.10 (0.00)	64.47 ± 1.25 (0.00)	0.00	857.21	27,673,154 (100%)
GA	✗	✓	98.37 ± 0.53 (1.30)	93.63 ± 0.46 (17.66)	72.36 ± 0.55 (2.67)	85.77 ± 1.10 (21.30)	10.73	7.92	27,673,154 (100%)
RL	✗	✓	97.56 ± 0.62 (2.11)	95.00 ± 1.64 (19.03)	70.57 ± 0.50 (4.46)	88.83 ± 0.99 (24.36)	12.49	7.61	27,673,154 (100%)
SalUn	✗	✓	98.47 ± 0.34 (1.20)	97.23 ± 1.01 (21.26)	71.86 ± 0.24 (3.17)	89.60 ± 1.08 (25.13)	12.69	12.79	13,836,577 (50%)
BT	✗	✓	96.46 ± 0.44 (3.21)	92.83 ± 0.92 (16.86)	69.52 ± 0.35 (5.51)	85.23 ± 0.78 (20.76)	11.59	8.23	27,673,154 (100%)
L2UL	✗	✓	94.77 ± 0.51 (4.90)	74.90 ± 0.10 (1.07)	68.69 ± 0.27 (6.34)	73.90 ± 0.46 (9.43)	5.44	7919.11	27,673,154 (100%)
COUN+RL	✗	✓	98.30 ± 0.32 (1.37)	96.47 ± 0.21 (20.50)	71.45 ± 0.26 (3.58)	89.02 ± 0.82 (24.55)	12.50	11.45	27,673,154 (100%)
DELETE	✗	✓	91.84 ± 2.12 (7.83)	77.57 ± 2.39 (1.60)	65.44 ± 1.43 (9.59)	68.67 ± 1.50 (4.20)	5.81	8.42	27,673,154 (100%)
LOFT	only $\Sigma_{\text{rm}}^{\text{pre}}$	only $\Sigma_{\text{fg}}^{\text{pre}}$	92.65 ± 0.54 (7.02)	82.97 ± 1.17 (7.00)	68.14 ± 0.42 (6.89)	64.47 ± 2.36 (0.00)	5.23	0.50	230,400 (0.83%)

forgetting $\mathcal{D}_{\text{fg}}^{\text{te}}$ and $\text{Acc}_{\text{rm}}^{\text{te}}$ on the remaining $\mathcal{D}_{\text{rm}}^{\text{te}}$ of the test data. In addition, the Membership Inference Attack (MIA) success rate (Shokri et al., 2017) is adopted, measuring the proportion of samples in \mathcal{D}_{fg} that gets memorized by the unlearned model. We mark the best results highlighted in bold font. Note that the performance gap to the retrained f_{exact} essentially reflects the unlearning efficacy of approximate MU methods. This is the key evaluation criterion for MU and is marked in blue within parentheses. Hence, the overall performances are indicated by the average of the accuracy and MIA gap to f_{exact} (Avg.G.).

5.2. Main Comparisons

Multi/Single-class unlearning. Tables 1 and 2 present comparisons on the unlearning results and computational costs with Swin-T on Tiny-ImageNet, where 4 of 200 classes are randomly selected as \mathcal{D}_{fg} . Table 1 shows that unlearning without access to \mathcal{D}_{rm} leads to substantial performance drops for baselines such as RL and SalUn, showing their strong reliance to \mathcal{D}_{rm} . Our LOFT leverages the two feature covariance matrices and achieves state-of-the-art unlearning performance with a smallest average gap of 0.85 to the retrained model. On efficiency, Table 2 shows that the parameter number and the Run Time Efficiency (RTE) in our LOFT are less by orders of magnitude than that of other baselines, as our subspace learning simply optimizes a projection matrix operating on two covariance matrices and others generally update the pretrained model with the original training data. For single-class unlearning, we consider the much more challenging ImageNet-1K dataset with ResNet50, where 1 of 1,000 classes is randomly selected as \mathcal{D}_{fg} with 3 repeated runs. Given the extremely large

scale of this dataset (\mathcal{D}_{rm} contains over 1.28M samples), we therefore compare with methods that only utilize \mathcal{D}_{fg} . The results in Table 3 demonstrates that LOFT outperforms other baselines with the smallest average gap, together with the shortest running time (less than 1 second) and the fewest number of parameters (reduced by approximately 96%).

Instance unlearning. LOFT is also applicable to instance-wise unlearning with results shown in Table 4, where 1,000 of 100,000 training samples (1%) in Tiny-ImageNet are randomly selected as \mathcal{D}_{fg} . Accuracy on the whole test dataset is evaluated as Acc_{te} . Under this random forgetting setting, \mathcal{D}_{fg} and \mathcal{D}_{rm} contain samples from all classes, which is more challenging to seek a feature subspace well differentiating \mathcal{D}_{fg} and \mathcal{D}_{rm} . Nevertheless, in Table 4, the low MIA gap of LOFT implies that its learned subspace can effectively remove information related to \mathcal{D}_{fg} . Furthermore, LOFT attains superior performance and efficiency on the overall Avg.G. metric across all baselines by optimizing only <1% parameters w.r.t. the given model in 0.5 seconds.

More unlearning setups, applications and generation tasks. Due to space limitation, we discuss two practical unlearning scenarios in Appendix D: *extreme unlearning* of forgetting a very high ratio of the training samples (deleting data from a large number of users) and *continual unlearning* with multiple unlearning requests in sequence. Additionally, we investigate MU in real-world applications, including *face recognition* and *emotion recognition*, in Appendix E. Our LOFT maintains superior performance across these unlearning setups and applications. Furthermore, Appendix F provides a preliminary exploration on the low-dimensional

Table 5. Ablation study on J_{rm} and J_{fg} .

objective	Acc ^{tr} _{rm}	Acc ^{tr} _{fg}	Acc ^{te} _{rm}	Acc ^{te} _{fg}	MIA
None	97.11	98.10	71.61	65.00	86.10
J_{fg} only	89.51	11.50	65.40	4.00	0.00
J_{rm} only	99.19	87.80	75.07	53.00	58.35
$J_{\text{rm}} + J_{\text{fg}}$	98.66	1.10	74.27	0.00	0.00

feature subspace for unlearning in generation tasks, while this field still remains underexplored. Our initial results suggest the potentials of LOFT for MU in generation tasks and offer beneficial insights for future work.

5.3. Ablation Study and Sensitivity Analysis

Objective terms J_{rm} and J_{fg} . We conduct experiments to explore the roles of the two loss terms in the optimization objective $J(\mathbf{U})$ of (2). These two terms together aim at the dual goals in MU: J_{rm} preserves performance on \mathcal{D}_{rm} and J_{fg} guarantees forgetting on \mathcal{D}_{fg} . By respectively removing J_{rm} and J_{fg} from $J(\mathbf{U})$, we report the results in Table 5. It shows that optimizing \mathbf{U} only with J_{fg} suppresses Acc_{fg} and MIA, while failing to preserve Acc_{rm} . Employing only J_{rm} manages to achieve high Acc_{rm} , but leaves \mathcal{D}_{fg} hardly forgotten with high Acc_{fg} and MIA. Hence, a joint optimization with both J_{rm} and J_{fg} is crucial for effective MU.

Subspace dimensions s . The projection matrix \mathbf{U} is confined on the Stiefel manifold $\text{St}(d, s)$, consisting of s orthonormal bases in columns. Here, the dimension s determines the captured feature information in the projected subspace. A sensitivity analysis w.r.t. varied values of s on the unlearning performance is provided in the left panel of Fig.3. As illustrated, there is a clear trade-off: a larger s preserves higher Acc_{rm} but sacrifices the ability to forget \mathcal{D}_{fg} and incurs higher computation, whereas a smaller s effectively forgets \mathcal{D}_{fg} but compromises Acc_{rm} . From our evaluations, we recommend initializing s with preserving 95% of the explained variance in $\Sigma_{\text{rm}}^{\text{pre}}$, as this choice readily provides good empirical performance for different settings and tasks evaluated in this work.

Implementation position for subspace learning. The subspace learning in our LOFT is primarily applied to the penultimate-layer features z , where the projection matrix \mathbf{U} is inserted between g_{pre} and h_{pre} . In practice, the implementation of LOFT is quite flexible to be inserted into different positions in f_{pre} . Here, we implement LOFT in different layers with f_{pre} exemplified on ResNet18, with results in Fig.3 (right). LOFT demonstrates flexibility by maintaining competitive performance when applied in earlier positions (layer1, layer2, layer3), compared to its default setting of layer4. It further indicates that the feature covariance matrices in earlier layers contain sufficient information

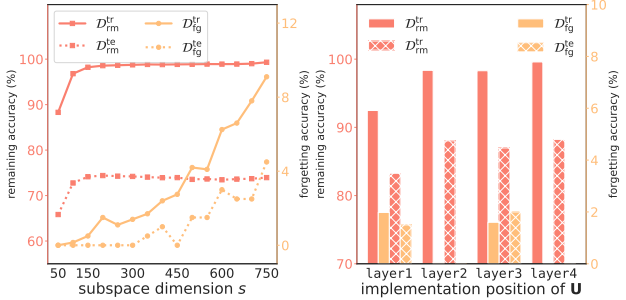


Figure 3. A sensitivity analysis on (i) subspace dimensions s (left) and (ii) different positions of the projection matrix \mathbf{U} (right).

to achieve effective MU from a low-dimensional feature subspace perspective. However, it can cost more computations, due to the larger feature dimensions and more optimization steps with early-layer implementation. Appendix C.4 provides detailed settings and related results on computations. Considering the trade-off between performance and efficiency, it is recommended to implement LOFT in the penultimate layer as done in main evaluations.

6. Conclusion and Discussion

This work presents a low-dimensional feature subspace perspective for MU, which is by far underexplored but shows great potentials with our evaluations. Our key insight lies in the promising separability between \mathcal{D}_{rm} and \mathcal{D}_{fg} in feature subspaces and seeks to learn such a subspace for the pre-trained model f_{pre} . Accordingly, we propose LOFT through PCA-based techniques to learn a projection matrix, thereby constructing a feature subspace that preserves the knowledge of \mathcal{D}_{rm} and diminishes that of \mathcal{D}_{fg} . In optimization, only one-shot feature fetching is required to compute the covariances, avoiding direct visits and massive reloads to raw training data for privacy protection. LOFT simply updates a small-size projection matrix and in implementation serves as a plug-in module to f_{pre} without modifying the entire parameters, which is of great practicality for handling multiple unlearning requests. LOFT reduces both the parameter number and the running time by orders of magnitude during training, while achieving superior unlearning accuracy, as supported by our extensive evaluations.

Since LOFT does not update the parameters of f_{pre} , it is not appropriate to be directly applied to generation tasks for MU, as the projection matrix needs to be carefully tailored to the specific generative model and its particular unlearning scenario. We primarily explore this direction in Appendix F with showing potentials of feature subspace learning for MU in generation tasks, which we hope could inspire sophisticated future investigations. Moreover, we provide in-depth discussions on some key aspects of LOFT in Appendix G, including the separability, scalability and privacy protection.

Impact Statement

This paper presents work aimed at advancing the privacy protection of modern deep learning models by integrating classic machine learning techniques. This advancement has the potential to benefit a wide range of fields and societal applications that are related to user privacy protection. By releasing our code along with this work, we aim to provide the machine unlearning research community with a fresh methodological perspective and an interpretable and practical plug-in module that can be optimized with superior effectiveness and efficiency. While we do not foresee direct negative societal impacts arising from this work, we intend to further refine and extend the method in future research.

References

Aljundi, R., Babiloni, F., Elhoseiny, M., Rohrbach, M., and Tuytelaars, T. Memory aware synapses: Learning what (not) to forget. In *European Conference on Computer Vision (ECCV)*, pp. 139–154, 2018.

Avron, H., Nguyen, H., and Woodruff, D. Subspace embeddings for the polynomial kernel. *Advances in Neural Information Processing Systems (NeurIPS)*, 27, 2014.

Becigneul, G. and Ganea, O.-E. Riemannian adaptive optimization methods. In *International Conference on Learning Representations (ICLR)*, 2019.

Bottou, L. Stochastic gradient descent tricks. In *Neural Networks: Tricks of the Trade: Second Edition*, pp. 421–436. Springer, 2012.

Bourtoule, L., Chandrasekaran, V., Choquette-Choo, C. A., Jia, H., Travers, A., Zhang, B., Lie, D., and Papernot, N. Machine unlearning. In *IEEE symposium on security and privacy (SP)*, pp. 141–159. IEEE, 2021.

Cao, Q., Shen, L., Xie, W., Parkhi, O. M., and Zisserman, A. VGGFACE2: A dataset for recognising faces across pose and age. In *IEEE International Conference on Automatic Face & Gesture Recognition*, pp. 67–74. IEEE, 2018.

Cao, Y. and Yang, J. Towards making systems forget with machine unlearning. In *IEEE Symposium on Security and Privacy*, pp. 463–480. IEEE, 2015.

Cha, S., Cho, S., Hwang, D., Lee, H., Moon, T., and Lee, M. Learning to unlearn: Instance-wise unlearning for pre-trained classifiers. In *AAAI conference on artificial intelligence*, volume 38, pp. 11186–11194, 2024.

Chen, T., Kornblith, S., Norouzi, M., and Hinton, G. A simple framework for contrastive learning of visual representations. In *International conference on machine learning*, pp. 1597–1607. PmLR, 2020.

Chundawat, V. S., Tarun, A. K., Mandal, M., and Kankanhalli, M. Can bad teaching induce forgetting? unlearning in deep networks using an incompetent teacher. In *AAAI Conference on Artificial Intelligence*, volume 37, pp. 7210–7217, 2023a.

Chundawat, V. S., Tarun, A. K., Mandal, M., and Kankanhalli, M. Zero-shot machine unlearning. *IEEE Transactions on Information Forensics and Security*, 18:2345–2354, 2023b.

Deng, J., Dong, W., Socher, R., Li, L.-J., Li, K., and Fei-Fei, L. Imagenet: A large-scale hierarchical image database. In *IEEE Conference on Computer Vision and Pattern Recognition (CVPR)*, pp. 248–255, 2009.

Dwork, C. Differential privacy. In *International colloquium on automata, languages, and programming*, pp. 1–12. Springer, 2006.

Fan, C., Liu, J., Zhang, Y., Wong, E., Wei, D., and Liu, S. Salun: Empowering machine unlearning via gradient-based weight saliency in both image classification and generation. In *International Conference on Learning Representations (ICLR)*, 2024.

Fang, K., Tao, Q., Lv, K., He, M., Huang, X., and YANG, J. Kernel pca for out-of-distribution detection. In *Advances in Neural Information Processing Systems (NeurIPS)*, volume 37, pp. 134317–134344, 2024.

Fu, C., Jia, W., and Ruan, N. Client-free federated unlearning via training reconstruction with anchor subspace calibration. In *ICASSP 2024-2024 IEEE International Conference on Acoustics, Speech and Signal Processing (ICASSP)*, pp. 9281–9285. IEEE, 2024.

Ginart, A., Guan, M., Valiant, G., and Zou, J. Y. Making ai forget you: Data deletion in machine learning. *Advances in Neural Information Processing Systems (NeurIPS)*, 32, 2019.

Golatkar, A., Achille, A., and Soatto, S. Eternal sunshine of the spotless net: Selective forgetting in deep networks. In *IEEE/CVF Conference on Computer Vision and Pattern Recognition*, pp. 9304–9312, 2020.

Graves, L., Nagisetty, V., and Ganesh, V. Amnesiac machine learning. In *AAAI Conference on Artificial Intelligence*, volume 35, pp. 11516–11524, 2021.

Guo, C., Goldstein, T., Hannun, A., and Van Der Maaten, L. Certified data removal from machine learning models. In *Proceedings of the 37th International Conference on Machine Learning*, volume 119 of *Proceedings of Machine Learning Research*, pp. 3832–3842. PMLR, 13–18 Jul 2020.

He, K., Zhang, X., Ren, S., and Sun, J. Deep residual learning for image recognition. In *IEEE Conference on Computer Vision and Pattern Recognition (CVPR)*, pp. 770–778, 2016.

Ho, J., Jain, A., and Abbeel, P. Denoising diffusion probabilistic models. *Advances in neural information processing systems*, 33:6840–6851, 2020.

Hoofnagle, C. J., Van Der Sloot, B., and Borgesius, F. Z. The european union general data protection regulation: what it is and what it means. *Information & Communications Technology Law*, 28(1):65–98, 2019.

Huang, Z., Cheng, X., Zheng, J., Wang, H., He, Z., Li, T., and Huang, X. Unified gradient-based machine unlearning with remain geometry enhancement. *Advances in Neural Information Processing Systems (NeurIPS)*, 37: 26377–26414, 2024.

Izzo, Z., Smart, M. A., Chaudhuri, K., and Zou, J. Approximate data deletion from machine learning models. In *International Conference on Artificial Intelligence and Statistics (AISTATS)*, pp. 2008–2016. PMLR, 2021.

Jia, J., Liu, J., Ram, P., Yao, Y., Liu, G., Liu, Y., Sharma, P., and Liu, S. Model sparsity can simplify machine unlearning. *Advances in Neural Information Processing Systems (NeurIPS)*, 36:51584–51605, 2023.

Khalil, Y. H., Setayesh, M., and Li, H. Coun: Empowering machine unlearning via contrastive learning. In *The Thirty-ninth Annual Conference on Neural Information Processing Systems*, 2025.

Kim, J. and Woo, S. S. Efficient two-stage model retraining for machine unlearning. In *IEEE/CVF Conference on Computer Vision and Pattern Recognition (CVPR)*, pp. 4361–4369, 2022.

Kochurov, M., Karimov, R., and Kozlukov, S. Geoopt: Riemannian optimization in pytorch. *arXiv preprint arXiv:2005.02819*, 2020.

Krizhevsky, A. Learning multiple layers of features from tiny images. *Master's thesis, University of Toronto*, 2009.

Kurmanji, M., Triantafillou, P., Hayes, J., and Triantafillou, E. Towards unbounded machine unlearning. *Advances in Neural Information Processing Systems (NeurIPS)*, 36: 1957–1987, 2023.

Le, Y. and Yang, X. Tiny imagenet visual recognition challenge. *CS 231N*, 7(7):3, 2015.

Li, G., Shen, L., Sun, Y., Hu, Y., Hu, H., and Tao, D. Subspace based federated unlearning. *arXiv preprint arXiv:2302.12448*, 2023a.

Li, S., Deng, W., and Du, J. Reliable crowdsourcing and deep locality-preserving learning for expression recognition in the wild. In *IEEE/CVF Conference on Computer Vision and Pattern Recognition (CVPR)*, pp. 2584–2593. IEEE, 2017.

Li, T., Tan, L., Huang, Z., Tao, Q., Liu, Y., and Huang, X. Low dimensional trajectory hypothesis is true: DNNs can be trained in tiny subspaces. *IEEE Transactions on Pattern Analysis and Machine Intelligence*, 45(3):3411–3420, 2023b.

Li, Z., Ye, Q., and Hu, H. Funu: Boosting machine unlearning efficiency by filtering unnecessary unlearning. In *ACM on Web Conference*, pp. 3366–3376, 2025.

Liu, J., Xue, M., Lou, J., Zhang, X., Xiong, L., and Qin, Z. Muter: Machine unlearning on adversarially trained models. In *IEEE/CVF Conference on Computer Vision and Pattern Recognition (CVPR)*, pp. 4892–4902, 2023.

Liu, S., Yao, Y., Jia, J., Casper, S., Baracaldo, N., Hase, P., Yao, Y., Liu, C. Y., Xu, X., Li, H., et al. Rethinking machine unlearning for large language models. *Nature Machine Intelligence*, pp. 1–14, 2025.

Liu, Y., Fan, M., Chen, C., Liu, X., Ma, Z., Wang, L., and Ma, J. Backdoor defense with machine unlearning. In *IEEE INFOCOM*, pp. 280–289, 2022.

Liu, Z., Lin, Y., Cao, Y., Hu, H., Wei, Y., Zhang, Z., Lin, S., and Guo, B. Swin transformer: Hierarchical vision transformer using shifted windows. In *IEEE/CVF International Conference on Computer Vision (ICCV)*, pp. 10012–10022, 2021.

Liu, Z., Wang, T., Huai, M., and Miao, C. Backdoor attacks via machine unlearning. In *AAAI Conference on Artificial Intelligence*, volume 38, pp. 14115–14123, 2024.

Lizzo, T. and Heck, L. Unlearn efficient removal of knowledge in large language models. In *Findings of the Association for Computational Linguistics: NAACL 2025*, pp. 7257–7268, 2025.

Loshchilov, I. and Hutter, F. Decoupled weight decay regularization. In *International Conference on Learning Representations (ICLR)*, 2019.

Madry, A., Makelov, A., Schmidt, L., Tsipras, D., and Vladu, A. Towards deep learning models resistant to adversarial attacks. In *International Conference on Learning Representations (ICLR)*, 2018.

Netzer, Y., Wang, T., Coates, A., Bissacco, A., Wu, B., and Ng, A. Y. Reading digits in natural images with unsupervised feature learning. In *NIPS Workshop on Deep Learning and Unsupervised Feature Learning*, 2011.

Pandey, A., Fanuel, M., Schreurs, J., and Suykens, J. A. K. Disentangled representation learning and generation with manifold optimization. *Neural Computation*, 34(10):2009–2036, 09 2022. ISSN 0899-7667. doi: 10.1162/neco_a_01528.

Papineni, K., Roukos, S., Ward, T., and Zhu, W.-J. Bleu: a method for automatic evaluation of machine translation. In *Proceedings of the 40th annual meeting of the Association for Computational Linguistics*, pp. 311–318, 2002.

Pearson, K. Liii. on lines and planes of closest fit to systems of points in space. *The London, Edinburgh, and Dublin philosophical magazine and journal of science*, 2(11): 559–572, 1901.

Peebles, W. and Xie, S. Scalable diffusion models with transformers. In *IEEE/CVF International Conference on Computer Vision (ICCV)*, pp. 4195–4205, 2023.

Rombach, R., Blattmann, A., Lorenz, D., Esser, P., and Ommer, B. High-resolution image synthesis with latent diffusion models. In *Proceedings of the IEEE/CVF conference on computer vision and pattern recognition*, pp. 10684–10695, 2022.

Schuhmann, C., Beaumont, R., Vencu, R., Gordon, C., Wightman, R., Cherti, M., Coombes, T., Katta, A., Mullis, C., Wortsman, M., et al. Laion-5b: An open large-scale dataset for training next generation image-text models. *Advances in Neural Information Processing Systems (NeurIPS)*, 35:25278–25294, 2022.

Sendera, M., Struski, Ł., Książek, K., Musiol, K., Tabor, J., and Rymarczyk, D. Semu: Singular value decomposition for efficient machine unlearning. *International Conference on Machine Learning (ICML)*, 2025.

Shokri, R., Stronati, M., Song, C., and Shmatikov, V. Membership inference attacks against machine learning models. In *IEEE Symposium on Security and Privacy (SP)*, pp. 3–18. IEEE, 2017.

Tarun, A. K., Chundawat, V. S., Mandal, M., and Kankanhalli, M. Fast yet effective machine unlearning. *IEEE Transactions on Neural Networks and Learning Systems*, 2023.

Thudi, A., Deza, G., Chandrasekaran, V., and Papernot, N. Unrolling sgd: Understanding factors influencing machine unlearning. In *IEEE European Symposium on Security and Privacy (EuroS&P)*, pp. 303–319. IEEE, 2022a.

Thudi, A., Jia, H., Shumailov, I., and Papernot, N. On the necessity of auditable algorithmic definitions for machine unlearning. In *USENIX Security Symposium*, pp. 4007–4022, 2022b.

Warnecke, A., Pirch, L., Wressnegger, C., and Rieck, K. Machine unlearning of features and labels. *arXiv preprint arXiv:2108.11577*, 2021.

Xiao, Y., Ye, Q., Hu, L., Zheng, H., Hu, H., Liang, Z., Li, H., and Jiao, Y. Reminiscence attack on residuals: Exploiting approximate machine unlearning for privacy. In *Proceedings of the IEEE/CVF International Conference on Computer Vision*, pp. 3058–3068, 2025.

Xu, X., Du, M., Ye, Q., and Hu, H. Obliviate: Robust and practical machine unlearning for large language models. In *EMNLP*, 2025.

Zha, D., Bhat, Z. P., Lai, K.-H., Yang, F., Jiang, Z., Zhong, S., and Hu, X. Data-centric artificial intelligence: A survey. *ACM Computing Surveys*, 57(5):1–42, 2025.

Zhou, Y., Zheng, D., Mo, Q., Lu, R., Lin, K.-Y., and Zheng, W.-S. Decoupled distillation to erase: A general unlearning method for any class-centric tasks. In *IEEE/CVF Conference on Computer Vision and Pattern Recognition (CVPR)*, pp. 20350–20359, 2025.

Appendices are organized as follows:

- Appendix A provides an overview of related work in machine unlearning and introduces the baseline MU methods included in our empirical comparisons.
- Appendix B contains proofs of Lemma 3.1 and Theorem 4.2 in the main text.
- Appendix C presents detailed setups of involved MU methods in experiments of *multi-class*, *single-class* and *instance-wise* unlearning in the main text, together with results about the implementation positions of LOFT.
- Appendix D supplements comparisons under two practical unlearning setups of *extreme unlearning* and *continual unlearning*.
- Appendix E supplements comparisons on machine unlearning under two real-world applications of *face recognition* and *emotion recognition*.
- Appendix F gives a preliminary exploration on the low-dimensional feature subspaces for MU in generation tasks.
- Appendix G discusses several key aspects of LOFT, including its separability, scalability, and implications for privacy protection.

A. Related Work on Machine Unlearning

Machine unlearning aims at maintaining prediction performances of a well-trained model f_{pre} when removing (forgetting) specific data (Cao & Yang, 2015; Ginart et al., 2019; Bourtoule et al., 2021). In general, such forgetting data \mathcal{D}_{fg} can mainly be categorized into *class-wise* and *instance-wise* types. The former indicates that \mathcal{D}_{fg} includes all the samples from one or multiple classes in \mathcal{Y} (Tarun et al., 2023; Chundawat et al., 2023b; Zhou et al., 2025) while the latter implies that \mathcal{D}_{fg} can be a random subset of the entire training data \mathcal{D} with mixed classes and even all classes (Kim & Woo, 2022; Fan et al., 2024; Cha et al., 2024).

A golden standard of MU is to retrain the model from scratch on the remaining data \mathcal{D}_{rm} only, known as *the exact MU* (Bourtoule et al., 2021; Thudi et al., 2022b). The resulting retrained model f_{exact} never sees the forgetting data \mathcal{D}_{fg} and thereby is an oracle in evaluating MU performance. However, the retraining of the given model on \mathcal{D}_{rm} can suffer from heavy computational overload, which motivates a series of researches optimizing the pretrained model f_{pre} by approaching to the ideal performance of the exact retrained model f_{exact} , namely *the approximate MU*. Existing approximate MU methods generally take different techniques to update f_{pre} , usually requiring to visit the forgetting data \mathcal{D}_{fg} and/or the remaining data \mathcal{D}_{rm} from the original training dataset. In the following, the involved MU methods in our comparisons are outlined, covering mainstream unlearning techniques and marking their reliance to \mathcal{D}_{fg} and \mathcal{D}_{rm} .

FT (Golatkar et al., 2020; Warnecke et al., 2021) fine-tunes the pretrained model f_{pre} only on the remaining data \mathcal{D}_{rm} via minimizing the cross-entropy loss exemplified on the classification task. In most cases, \mathcal{D}_{fg} only accounts for a small proportion of the entire training set, and thereby the time consuming for FT per epoch remains relatively high.

GA (Graves et al., 2021; Thudi et al., 2022a) fine-tunes f_{pre} by applying gradient ascent only on the forgetting data \mathcal{D}_{fg} , implemented by maximizing the cross entropy loss. GA is highly sensitive to the learning rate and usually leads to a substantial drop on the performance of \mathcal{D}_{rm} .

RL (Golatkar et al., 2020) fine-tunes f_{pre} by replacing the labels of \mathcal{D}_{fg} with new different random labels. RL is implemented with both \mathcal{D}_{fg} and \mathcal{D}_{rm} involved and can easily approach the performance of the ideal retrained model f_{exact} . Nevertheless, existing researches have highlighted the importance of MU with only \mathcal{D}_{fg} accessible (Cha et al., 2024; Zhou et al., 2025). Under this more practical setting with limited data access, RL excluding \mathcal{D}_{rm} in optimization shows unsatisfactory accuracy on \mathcal{D}_{rm} and \mathcal{D}_{fg} , verified by our empirical results in this work.

SalUn (Fan et al., 2024) proposes to mask those parameters in f_{pre} that are sensitive to \mathcal{D}_{fg} . In implementation, a parameter saliency mask is derived based on \mathcal{D}_{fg} only, and then is applied to the fine-tuning of f_{pre} . The fine-tuning of SalUn follows RL and similarly faces the aforementioned challenge as RL. SalUn excluding \mathcal{D}_{rm} in the fine-tuning shows uncompetitive unlearning results and the saliency mask does not bring significant performance gains to RL when \mathcal{D}_{fg} is only available. Another technique with a similar idea of leveraging parameter sparsity is applying an additional ℓ_1 regularization on the parameters of f_{pre} based on RL (Jia et al., 2023). Besides SalUn, SFR-on (Huang et al., 2024) further introduces gradient

information via Hessians into the parameter mask and proposes a unified optimization framework with a fast-slow weight update. SFR-on also heavily relies on \mathcal{D}_{rm} in computing the Fisher information matrix and the loss function.

BT (Chundawat et al., 2023a) introduces knowledge distillation for approximated MU. There are two teacher models in BT: an incompetent teacher model being a randomly-initialized network and a competent teacher model being the pretrained model f_{pre} . The student model is also the pretrained network f_{pre} . During unlearning, the competent/incompetent teacher distills information from $\mathcal{D}_{\text{rm}}/\mathcal{D}_{\text{fg}}$ to the student via the KL divergence. The competent teacher and the student actually share the same network in memory, implying that the competent teacher gets updated during distillation. Although both \mathcal{D}_{rm} and \mathcal{D}_{fg} are involved, our experiments show that BT solely with \mathcal{D}_{fg} , i.e., a single incompetent teacher, still achieves good results. SCRUB (Kurmanji et al., 2023) is also based on distillation, with the pretrained model as the teacher. In SCRUB, the pretrained model is optimized under the guidance of the teacher by minimizing/maximizing the KL divergence with $\mathcal{D}_{\text{rm}}/\mathcal{D}_{\text{fg}}$ and a cross-entropy loss on \mathcal{D}_{rm} .

L2UL (Cha et al., 2024) introduces adversarial examples (AEs) (Madry et al., 2018) and weight importance (Aljundi et al., 2018) to promote MU given access only to \mathcal{D}_{fg} . As claimed in L2UL, AEs w.r.t. \mathcal{D}_{fg} can mimic the remaining data \mathcal{D}_{rm} , so that minimizing the cross-entropy loss on those AEs can benefit the performance on \mathcal{D}_{rm} . A parameter importance mask is further applied, where changes of weights that are less important in classifying \mathcal{D}_{fg} get penalized. L2UL is particularly superior in instance-wise unlearning. However, the computational demand of L2UL is prohibitively heavy. Generating AEs with its default configuration (100 iterations, 200 AEs/image) for a dataset as large as ImageNet-1K (over 1.28M training images) renders the approach impractical.

COUN (Khalil et al., 2025) leverages the contrastive learning (Chen et al., 2020) for MU. COUN basically follows FT, i.e., fine-tunes f_{pre} by supervised training only on the remaining data \mathcal{D}_{rm} , and adds an additional contrastive learning loss on \mathcal{D}_{rm} . The rationale behind is to implicitly push forgetting representations towards those remaining representations with the highest semantic similarity by regularizing the augmented views of \mathcal{D}_{rm} via the contrastive loss. As originally reported, COUN is trained solely on \mathcal{D}_{rm} and improves unlearning performance over FT. To explore whether its contrastive learning paradigm can consistently enhance performance when only \mathcal{D}_{fg} is available, we adapt COUN to operate with the RL method using only \mathcal{D}_{fg} , denoted as “COUN+RL” in our comparisons. Under this restricted data access, the contrastive learning implemented in COUN brings limited performance gains, as demonstrated in our results.

DELETE (Zhou et al., 2025) is a distillation-based method relying only on \mathcal{D}_{fg} . In DELETE, a copy of the pretrained network is utilized as the teacher model, and the key is to apply a mask to the outputs from the teacher. This mask aims at altering the predictive probabilities of \mathcal{D}_{fg} to approximate the ideal case and is implemented in a simple way: positions in the mask w.r.t. the ground-truth labels of \mathcal{D}_{fg} are set to negative infinity and others are set to zero.

Beyond the baselines previously discussed, we further review several subspace-based MU methods that are more closely relevant with our LOFT. These methods typically define their subspaces in a *non-learnable* way based on network *parameters*. Gradient subspaces in convolution neural networks are identified in (Li et al., 2023a; Fu et al., 2024) through eigen-decomposition. In (Lizzo & Heck, 2025), the subspace in large language models is constructed by applying the Gram-Schmidt process to the singular vectors of parameters. A latest unlearning method SEMU (Sendera et al., 2025) performs SVD disentanglement on the gradients of \mathcal{D}_{fg} to identify and update parameters mostly important for unlearning. However, our empirical results show that SEMU yields poor unlearning performance on SwinT. This limitation possibly stems from the fact that its decomposition, applied to parameters of 2d convolution and linear layers, may not adequately adapt to the attention structure in transformers. Thereby we omit comparisons with SEMU. In contrast, our LOFT fundamentally differs from these methods by leveraging a *learnable feature subspace* for unlearning.

Researches in MU have been extended to a wide range of fields with different tasks. The class-wise and concept forgetting in image generation is explored in (Fan et al., 2024; Huang et al., 2024). Privacy attacks against MU methods and corresponding defenses are discussed in (Xiao et al., 2025). Unlearning from adversarially trained models is exploited to achieve superior unlearning performance and also strong adversarial robustness (Liu et al., 2023). The concept of unnecessary unlearning is formalized in (Li et al., 2025) with an algorithm to filter those unnecessary requests. MU can be an effective tool for defending the backdoor attacks (Liu et al., 2022; 2024) through forgetting the backdoor triggers hidden in data. Moreover, MU in large language models has also received significant attention with extensive researches in recent years (Xu et al., 2025; Liu et al., 2025).

B. Proofs

B.1. Proof of Lemma 3.1

Proof. The ideal unlearning model f_{exact} is trained solely on the remaining data \mathcal{D}_{rm} , such that f_{exact} sufficiently learns knowledge from \mathcal{D}_{rm} and has never seen the forgetting data \mathcal{D}_{fg} . We thereby assume that the remaining features $\mathbf{Z}_{\text{fg}}^{\text{exact}}$ learned by the backbone of f_{exact} satisfy that the variance of $\mathbf{Z}_{\text{rm}}^{\text{exact}}$ is distributed compactly. That is, for the eigenvalues $\lambda_1 \geq \lambda_2 \geq \dots \geq \lambda_d > 0$ of $\Sigma_{\text{rm}}^{\text{exact}} \in \mathbb{R}^{d \times d}$, there exists a small positive integer s such that $s \ll d$, we have $\frac{\sum_{i=1}^s \lambda_i}{\sum_{i=1}^d \lambda_i} \geq 1 - \xi$, where $\xi > 0$ is a very small positive number, e.g. $\xi = 0.05$.

For any feature $\mathbf{z}_{\text{rm}}^{\text{exact}}$ of \mathcal{D}_{rm} from g_{exact} , we have:

$$\mathbb{E} [\|(\mathbf{I} - \mathbf{U}_* \mathbf{U}_*^\top)(\mathbf{z}_{\text{rm}}^{\text{exact}} - \boldsymbol{\mu}_{\text{rm}}^{\text{exact}})\|_2^2] = \sum_{i=s+1}^d \lambda_i = \xi \cdot \text{Tr}(\Sigma_{\text{rm}}^{\text{exact}}), \quad (3)$$

where $\boldsymbol{\mu}_{\text{rm}}^{\text{exact}}$ denotes the means of $\mathbf{Z}_{\text{rm}}^{\text{exact}}$. Therefore, $\|(\mathbf{I} - \mathbf{U}_* \mathbf{U}_*^\top)g_{\text{exact}}(\mathbf{x})\|_2 \leq \epsilon_{\text{rm}}$ for $\mathbf{x} \in \mathcal{D}_{\text{rm}}$ holds with $\epsilon_{\text{rm}} \propto \sqrt{\xi}$.

Similarly, for any features $\mathbf{z}_{\text{fg}}^{\text{exact}}$ of \mathcal{D}_{fg} from g_{exact} , we have:

$$\begin{aligned} \|\mathbf{U}_* \mathbf{U}_*^\top \mathbf{z}_{\text{fg}}^{\text{exact}}\|_2^2 &= \|\mathbf{U}_* \mathbf{U}_*^\top (\boldsymbol{\mu}_{\text{fg}}^{\text{exact}} + \mathbf{z}_{\text{fg}}^{\text{exact}} - \boldsymbol{\mu}_{\text{fg}}^{\text{exact}})\|_2^2 \\ &\leq (\|\mathbf{U}_* \mathbf{U}_*^\top \boldsymbol{\mu}_{\text{fg}}^{\text{exact}}\|_2 + \|\mathbf{U}_* \mathbf{U}_*^\top (\mathbf{z}_{\text{fg}}^{\text{exact}} - \boldsymbol{\mu}_{\text{fg}}^{\text{exact}})\|_2)^2. \end{aligned} \quad (4)$$

We can assume the boundedness of feature means: $\|\boldsymbol{\mu}_{\text{fg}}^{\text{exact}}\|_2 \leq M_{\boldsymbol{\mu}}$. Since \mathbf{U}_* is derived from \mathcal{D}_{rm} , and $\boldsymbol{\mu}_{\text{fg}}^{\text{exact}}$ comes from data that are not involved during the training of f_{exact} , we introduce a coefficient α to measure the alignment between $\boldsymbol{\mu}_{\text{fg}}^{\text{exact}}$ and the subspace \mathbf{U}_* : $\|\mathbf{U}_* \mathbf{U}_*^\top \boldsymbol{\mu}_{\text{fg}}^{\text{exact}}\|_2 \leq \alpha \cdot \|\boldsymbol{\mu}_{\text{fg}}^{\text{exact}}\|_2 \leq \alpha_{\max} \cdot M_{\boldsymbol{\mu}}$ with an upper bound α_{\max} for α .

Besides, the expectation of $\|\mathbf{U}_* \mathbf{U}_*^\top (\mathbf{z}_{\text{fg}}^{\text{exact}} - \boldsymbol{\mu}_{\text{fg}}^{\text{exact}})\|_2$ is given by

$$\begin{aligned} \mathbb{E} [\|\mathbf{U}_* \mathbf{U}_*^\top (\mathbf{z}_{\text{fg}}^{\text{exact}} - \boldsymbol{\mu}_{\text{fg}}^{\text{exact}})\|_2^2] &= \mathbb{E} [(\mathbf{z}_{\text{fg}}^{\text{exact}} - \boldsymbol{\mu}_{\text{fg}}^{\text{exact}})^\top \mathbf{U}_* \mathbf{U}_*^\top (\mathbf{z}_{\text{fg}}^{\text{exact}} - \boldsymbol{\mu}_{\text{fg}}^{\text{exact}})] \\ &= \text{Tr}(\mathbf{U}_*^\top \Sigma_{\text{fg}}^{\text{exact}} \mathbf{U}_*). \end{aligned} \quad (5)$$

We denote σ_{\max}^2 to bound the maximal projection variance: $\|\Sigma_{\text{fg}}^{\text{exact}}{}^{1/2} \mathbf{U}_*\|_2^2 \leq \sigma_{\max}^2$, and then we have $\|\mathbf{U}_* \mathbf{U}_*^\top (\mathbf{z}_{\text{fg}}^{\text{exact}} - \boldsymbol{\mu}_{\text{fg}}^{\text{exact}})\|_2 \leq \sqrt{s} \cdot \sigma_{\max} + \mathcal{O}(1)$. Therefore, $\forall \mathbf{x} \in \mathcal{D}_{\text{fg}}$, $\|\mathbf{U}_* \mathbf{U}_*^\top g_{\text{exact}}(\mathbf{x})\|_2 \leq \epsilon_{\text{fg}}$ holds for $\epsilon_{\text{fg}} = \alpha_{\max} \cdot M_{\boldsymbol{\mu}} + \sqrt{s} \cdot \sigma_{\max} + \mathcal{O}(1)$. The proof finishes. \square

Remark B.1. We particularly discuss the scenarios when \mathcal{D}_{fg} and \mathcal{D}_{rm} share high similarities. In this case, the exact MU model f_{exact} , though trained on \mathcal{D}_{rm} only, inevitably encode partial knowledge of \mathcal{D}_{fg} . Correspondingly, in our proof above, the projection matrix \mathbf{U}_* from the eigen-decomposition on $\mathbf{Z}_{\text{rm}}^{\text{exact}}$ also contains variance of $\mathbf{Z}_{\text{fg}}^{\text{exact}}$, resulting in larger upper bounds α_{\max} and σ_{\max} for the alignment coefficient α and the projection variance $\|\Sigma_{\text{fg}}^{\text{exact}}{}^{1/2} \mathbf{U}_*\|_2^2$. Then, the bound ϵ_{fg} for $\|\mathbf{U}_* \mathbf{U}_*^\top g_{\text{exact}}(\mathbf{x})\|_2$ becomes even looser, and the separability of \mathbf{U}_* might be less effective.

B.2. Proof of Theorem 4.2

We firstly present the assumptions required for the proof of Theorem 4.2.

Assumption B.2. The pretrained network f_{pre} and the retrained network f_{exact} differ in whether the forgetting data are involved into training, and show nearly the same performance on the remaining data. In this sense, for any $\mathbf{x} \in \mathcal{D}$, we can assume that differences in their learned features are bounded: $\|g_{\text{pre}}(\mathbf{x}) - g_{\text{exact}}(\mathbf{x})\|_2 \leq \epsilon_d$, and the output features of f_{exact} are assumed to be bounded as $\|g_{\text{exact}}(\mathbf{x})\|_2 \leq \epsilon_{\text{exact}}$.

Assumption B.3. The last linear layer $h_{\text{pre}}(\cdot)$ in the pretrained network f_{pre} is L_{pre} -Lipschitz continuous:

$$\|h_{\text{pre}}(\mathbf{z}_1) - h_{\text{pre}}(\mathbf{z}_2)\|_2 \leq L_{\text{pre}} \cdot \|\mathbf{z}_1 - \mathbf{z}_2\|_2, \quad \forall \mathbf{z}_1, \mathbf{z}_2 \in \mathbb{R}^d. \quad (6)$$

Specifically, the linear layer $h_{\text{pre}}(\cdot)$ with parameters \mathbf{W}_{pre} , i.e., $h_{\text{pre}}(\mathbf{z}) = \mathbf{W}_{\text{pre}}^\top \mathbf{z}$, has the Lipschitz constant $L_{\text{pre}} = \|\mathbf{W}_{\text{pre}}\|_2$. Similarly, the linear layer h_{exact} in the exact MU model f_{exact} has the Lipschitz constant $L_{\text{exact}} = \|\mathbf{W}_{\text{exact}}\|_2$ with its parameters $\mathbf{W}_{\text{exact}}$. We assume that the difference between parameters \mathbf{W}_{pre} and $\mathbf{W}_{\text{exact}}$ is bounded by $\|\mathbf{W}_{\text{pre}} - \mathbf{W}_{\text{exact}}\|_2 \leq \epsilon_W$.

The proof of Theorem 4.2 is given below.

Proof. We consider two cases that the input \mathbf{x} is from \mathcal{D}_{rm} and \mathcal{D}_{fg} , respectively. For any data $\mathbf{x} \in \mathcal{D}_{\text{rm}}$, we have:

$$\begin{aligned} \|f_{\hat{\mathbf{U}}}(\mathbf{x}) - f_{\text{exact}}(\mathbf{x})\|_2 &\leq \|h_{\text{pre}}(\hat{\mathbf{U}}\hat{\mathbf{U}}^\top g_{\text{pre}}(\mathbf{x})) - h_{\text{pre}}(\hat{\mathbf{U}}\hat{\mathbf{U}}^\top g_{\text{exact}}(\mathbf{x}))\|_2 \\ &\quad + \|h_{\text{pre}}(\hat{\mathbf{U}}\hat{\mathbf{U}}^\top g_{\text{exact}}(\mathbf{x})) - h_{\text{pre}}(g_{\text{exact}}(\mathbf{x}))\|_2 \\ &\quad + \|h_{\text{pre}}(g_{\text{exact}}(\mathbf{x})) - h_{\text{exact}}(g_{\text{exact}}(\mathbf{x}))\|_2. \end{aligned} \quad (7)$$

We denote the 3 terms in Eqn.(7) as follows:

$$\begin{aligned} A &= \|h_{\text{pre}}(\hat{\mathbf{U}}\hat{\mathbf{U}}^\top g_{\text{pre}}(\mathbf{x})) - h_{\text{pre}}(\hat{\mathbf{U}}\hat{\mathbf{U}}^\top g_{\text{exact}}(\mathbf{x}))\|_2, \\ B &= \|h_{\text{pre}}(\hat{\mathbf{U}}\hat{\mathbf{U}}^\top g_{\text{exact}}(\mathbf{x})) - h_{\text{pre}}(g_{\text{exact}}(\mathbf{x}))\|_2, \\ C &= \|h_{\text{pre}}(g_{\text{exact}}(\mathbf{x})) - h_{\text{exact}}(g_{\text{exact}}(\mathbf{x}))\|_2. \end{aligned} \quad (8)$$

These 3 terms A , B and C are bounded, respectively as follows:

$$\begin{aligned} A &= \|h_{\text{pre}}(\hat{\mathbf{U}}\hat{\mathbf{U}}^\top g_{\text{pre}}(\mathbf{x})) - h_{\text{pre}}(\hat{\mathbf{U}}\hat{\mathbf{U}}^\top g_{\text{exact}}(\mathbf{x}))\|_2 \\ &\leq L_{\text{pre}} \cdot \|\hat{\mathbf{U}}\hat{\mathbf{U}}^\top(g_{\text{pre}}(\mathbf{x}) - g_{\text{exact}}(\mathbf{x}))\|_2 \quad (\text{Assumption B.3}) \\ &\leq L_{\text{pre}} \cdot \|\hat{\mathbf{U}}\hat{\mathbf{U}}^\top\|_2 \cdot \|g_{\text{pre}}(\mathbf{x}) - g_{\text{exact}}(\mathbf{x})\|_2 \\ &\leq L_{\text{pre}} \cdot \epsilon_d, \quad (\text{Assumption B.2}) \end{aligned} \quad (9)$$

$$\begin{aligned} B &= \|h_{\text{pre}}(\hat{\mathbf{U}}\hat{\mathbf{U}}^\top g_{\text{exact}}(\mathbf{x})) - h_{\text{pre}}(g_{\text{exact}}(\mathbf{x}))\|_2 \\ &\leq L_{\text{pre}} \cdot \|(\mathbf{I} - \hat{\mathbf{U}}\hat{\mathbf{U}}^\top)g_{\text{exact}}(\mathbf{x})\|_2 \quad (\text{Assumption B.3}) \\ &\leq L_{\text{pre}} \cdot (\|(\mathbf{I} - \mathbf{U}_* \mathbf{U}_*^\top)g_{\text{exact}}(\mathbf{x})\|_2 + \|(\mathbf{U}_* \mathbf{U}_*^\top - \hat{\mathbf{U}}\hat{\mathbf{U}}^\top)g_{\text{exact}}(\mathbf{x})\|_2) \\ &\leq L_{\text{pre}} \cdot (\epsilon_{\text{rm}} + \|\mathbf{U}_* \mathbf{U}_*^\top - \hat{\mathbf{U}}\hat{\mathbf{U}}^\top\|_F \cdot \|g_{\text{exact}}(\mathbf{x})\|_2) \quad (\text{Lemma 3.1}) \\ &\leq L_{\text{pre}} \cdot (\epsilon_{\text{rm}} + \mathcal{O}(\epsilon_{\text{opt}})), \end{aligned} \quad (10)$$

where ϵ_{rm} is from the Lemma 3.1, and $C = \|h_{\text{pre}}(g_{\text{exact}}(\mathbf{x})) - h_{\text{exact}}(g_{\text{exact}}(\mathbf{x}))\|_2 \leq \|\mathbf{W}_{\text{pre}} - \mathbf{W}_{\text{exact}}\|_2 \cdot \|g_{\text{exact}}(\mathbf{x})\|_2 \leq \epsilon_W \cdot \epsilon_{\text{exact}}$ according to Assumption B.3.

Similarly, for any data $\mathbf{x} \in \mathcal{D}_{\text{fg}}$, we conduct decomposition on $\|f_{\hat{\mathbf{U}}}(\mathbf{x}) - f_{\text{exact}}(\mathbf{x})\|_2$, such that

$$\begin{aligned} \|f_{\hat{\mathbf{U}}}(\mathbf{x}) - f_{\text{exact}}(\mathbf{x})\|_2 &\leq \|h_{\text{pre}}(\hat{\mathbf{U}}\hat{\mathbf{U}}^\top g_{\text{pre}}(\mathbf{x})) - h_{\text{pre}}(\hat{\mathbf{U}}\hat{\mathbf{U}}^\top g_{\text{exact}}(\mathbf{x}))\|_2 \\ &\quad + \|h_{\text{pre}}(\hat{\mathbf{U}}\hat{\mathbf{U}}^\top g_{\text{exact}}(\mathbf{x})) - h_{\text{pre}}(\mathbf{0})\|_2 \\ &\quad + \|h_{\text{pre}}(\mathbf{0}) - h_{\text{exact}}(g_{\text{exact}}(\mathbf{x}))\|_2, \end{aligned} \quad (11)$$

where $\mathbf{0}$ denotes a d -dimensional all-zero vector. We denote $B_1 = \|h_{\text{pre}}(\hat{\mathbf{U}}\hat{\mathbf{U}}^\top g_{\text{exact}}(\mathbf{x})) - h_{\text{pre}}(\mathbf{0})\|_2$ and $C_1 = \|h_{\text{pre}}(\mathbf{0}) - h_{\text{exact}}(g_{\text{exact}}(\mathbf{x}))\|_2$, which are given by

$$\begin{aligned} B_1 &= \|h_{\text{pre}}(\hat{\mathbf{U}}\hat{\mathbf{U}}^\top g_{\text{exact}}(\mathbf{x})) - h_{\text{pre}}(\mathbf{0})\|_2 \\ &\leq L_{\text{pre}} \cdot \|\hat{\mathbf{U}}\hat{\mathbf{U}}^\top g_{\text{exact}}(\mathbf{x})\|_2 \quad (\text{Assumption B.3}) \\ &\leq L_{\text{pre}} \cdot (\|\mathbf{U}_* \mathbf{U}_*^\top g_{\text{exact}}(\mathbf{x})\|_2 + \|(\hat{\mathbf{U}}\hat{\mathbf{U}}^\top - \mathbf{U}_* \mathbf{U}_*^\top)g_{\text{exact}}(\mathbf{x})\|_2) \\ &\leq L_{\text{pre}} \cdot (\epsilon_{\text{fg}} + \mathcal{O}(\epsilon_{\text{opt}})), \end{aligned} \quad (12)$$

where ϵ_{fg} is from the Lemma 3.1, and $C_1 = \|h_{\text{pre}}(\mathbf{0}) - h_{\text{exact}}(g_{\text{exact}}(\mathbf{x}))\|_2 \leq L_{\text{exact}} \cdot \epsilon_{\text{exact}}$ according to Assumption B.2 and Assumption B.3.

Therefore, given $\mathbf{x} \in \mathcal{D}$, the difference in outputs between $f_{\hat{\mathbf{U}}}$ and f_{exact} is bounded by $\|f_{\hat{\mathbf{U}}}(\mathbf{x}) - f_{\text{exact}}(\mathbf{x})\|_2 \leq L_{\text{pre}} \cdot (\epsilon_d + \max(\epsilon_{\text{fg}}, \epsilon_{\text{rm}}) + \mathcal{O}(\epsilon_{\text{opt}})) + \epsilon_{\text{exact}} \cdot \max(L_{\text{exact}}, \epsilon_W)$. \square

Table S1. Training hyper-parameters of different MU methods w.r.t. results of multi-class unlearning in Table 1 with Swin-T on Tiny-ImageNet.

method	\mathcal{D}_{rm}	\mathcal{D}_{fg}	hyper-parameters
pretrained	✓	✓	20 epochs, lr = 10^{-4} , cosine scheduler
retrained	✓	✗	20 epochs, lr = 10^{-4} , cosine scheduler
FT	✓	✗	10 epochs, lr = 10^{-4} , cosine scheduler
GA	✗	✓	10 epochs, lr = 2×10^{-6} , constant scheduler
RL	✗	✓	10 epochs, lr = 10^{-5} , cosine scheduler
RL	✓	✓	10 epochs, lr = 10^{-4} , cosine scheduler
SalUn	✗	✓	10 epochs, lr = 10^{-5} , cosine scheduler, saliency sparsity 50%
SalUn	✓	✓	10 epochs, lr = 10^{-4} , cosine scheduler, saliency sparsity 50%
BT	✗	✓	10 epochs, lr = 10^{-5} , cosine scheduler, temperature scalar = 1.0
L2UL	✗	✓	lr = 10^{-5} , constant scheduler, regularization coefficient = 1.0
COUN+RL	✗	✓	10 epochs, lr = 2×10^{-5} , cosine scheduler
DELETE	✗	✓	10 epochs, lr = 10^{-5} , cosine scheduler
LOFT	only $\Sigma_{\text{rm}}^{\text{pre}}$	only $\Sigma_{\text{fg}}^{\text{pre}}$	50 steps, $s = 250$, lr = 1, constant scheduler

C. Implementation Details of Experiments in Main Text

C.1. Training Details of Multi-Class Unlearning

For multi-class unlearning in Table 1 with Swin-T on Tiny-ImageNet, we adopt the PyTorch-released checkpoint trained on ImageNet-1K as a starting point, and fine-tune this checkpoint on Tiny-ImageNet to obtain the pretrained model. In the repeated 3 experiments of Table 1, the randomly selected 4 forgetting labels (classes) are {11, 83, 115, 153}, {44, 65, 150, 168} and {53, 57, 108, 179}, respectively. All compared methods use the AdamW optimizer (Loshchilov & Hutter, 2019) with a weight decay of 0.05 and a batch size of 128. In L2UL (Cha et al., 2024), to generate adversarial examples, the ℓ_2 -PGD targeted attack is employed with a step size of 0.1, a perturbation bound of 0.4 and 100 iteration steps, and 200 adversarial examples are generated per image. The termination of the L2UL unlearning is carefully selected until the accuracy on the training forgetting data is sufficiently low without a substantial accuracy drop on the training remaining data. All the training hyper-parameters to obtain results in Table 1 are listed in Table S1. Our LOFT adopts the Riemannian Adam optimizer (Kochurov et al., 2020) for the projection matrix \mathbf{U} with a weight decay of 0.05, where the penultimate layer feature dimension with Swin-T on Tiny-ImageNet is $d = 768$.

C.2. Training Details of Single-Class Unlearning

For single-class unlearning in Table 3 with ResNet50 on ImageNet-1K, we deploy the PyTorch-released checkpoint that is exactly pretrained on ImageNet-1K as the pretrained model f_{pre} . Regarding the retrained model f_{exact} for unlearning, we train ResNet50 from scratch on the remaining data \mathcal{D}_{rm} for 90 epochs on 4 NVIDIA GeForce RTX 4090 GPUs, which runs for around 24 hours. In the repeated 3 experiments of Table 3, the randomly selected forgetting labels are 97, 316, and 852, respectively. All the compared methods use the SGD optimizer (Bottou, 2012) with a weight decay of 1×10^{-4} , the momentum of 0.9, and a batch size of 128. All the training hyper-parameters for the results in Table 3 are listed Table S2. Our LOFT keeps the settings of using the Riemannian Adam optimizer (Kochurov et al., 2020) for \mathbf{U} with a weight decay of 0.05, where the penultimate layer feature dimension with ResNet50 on ImageNet-1K is $d = 2048$.

C.3. Training Details of Instance Unlearning

For instance unlearning in Table 4 with Swin-T on Tiny-ImageNet, the basic settings are with that in Sec. C.1. 1,000 samples from the total 100,000 training samples are randomly selected as the forgetting data \mathcal{D}_{fg} (1%). Each of the repeated 3 experiments of Table 4 is corresponding to different random seeds, i.e., 0, 1 and 2. All compared methods use the AdamW optimizer (Loshchilov & Hutter, 2019) with a weight decay of 0.05 and a batch size of 128. The hyper-parameters are listed in Table S3. Our LOFT uses the Riemannian Adam optimizer (Kochurov et al., 2020) with a weight decay of 0.05.

Table S2. Training hyper-parameters of different MU methods w.r.t. results of single-class unlearning in Table 3 with ResNet50 on ImageNet-1K.

method	\mathcal{D}_{rm}	\mathcal{D}_{fg}	hyper-parameters
pretrained	✓	✓	-
retrained	✓	✗	90 epochs, lr = 10^{-1} , LR decay: 0.1 every 30 epochs
GA	✗	✓	3 epochs, lr = 10^{-4} , constant scheduler
RL	✗	✓	5 epochs, lr = 5×10^{-5} , cosine scheduler
SalUn	✗	✓	10 epochs, lr = 10^{-4} , cosine scheduler, saliency sparsity 50%
BT	✗	✓	5 epochs, lr = 1×10^{-5} , cosine scheduler, temperature scalar = 1.0
COUN+RL	✗	✓	3 epochs, lr = 10^{-6} , cosine scheduler
DELETE	✗	✓	5 epochs, lr = 10^{-1} , cosine scheduler
LOFT	only Σ_{rm}^{pre}	only Σ_{fg}^{pre}	100 steps, s = 500, lr = 10, constant scheduler

Table S3. Training hyper-parameters of different MU methods w.r.t. results of instance unlearning in Table 4 with Swin-T on Tiny-ImageNet.

method	\mathcal{D}_{rm}	\mathcal{D}_{fg}	hyper-parameters
pretrained	✓	✓	20 epochs, lr = 10^{-4} , cosine scheduler
retrained	✓	✗	20 epochs, lr = 10^{-4} , cosine scheduler
GA	✗	✓	10 epochs, lr = 6×10^{-6} , constant scheduler
RL	✗	✓	10 epochs, lr = 10^{-5} , cosine scheduler
SalUn	✗	✓	10 epochs, lr = 10^{-5} , cosine scheduler, saliency sparsity 50%
BT	✗	✓	10 epochs, lr = 10^{-5} , cosine scheduler, temperature scalar = 1.0
L2UL	✗	✓	lr = 10^{-4} , constant scheduler, regularization coefficient = 1.0
COUN+RL	✗	✓	10 epochs, lr = 10^{-5} , cosine scheduler
DELETE	✗	✓	10 epochs, lr = 2×10^{-5} , cosine scheduler
LOFT	only Σ_{rm}^{pre}	only Σ_{fg}^{pre}	100 steps, s = 300, lr = 1, constant scheduler

C.4. Implementation Positions for Subspace Learning

As discussed in Sec.5.3 of the main text, LOFT is implemented in different layers with f_{pre} exemplified on ResNet18. Specifically, ResNet18 is structured with a preceding module followed by 4 layer modules (layer1, layer2, layer3 and layer4) and a linear layer module¹. By default, LOFT is applied to the penultimate-layer features, i.e., features after the layer4 module. In experiments, we further apply LOFT to earlier layer modules (layer1, layer2 and layer3) to investigate the unlearning effectiveness of subspace learning at such positions, with results shown in the right panel of Fig.3 with ResNet18 on CIFAR10.

As shown in Fig.3, our LOFT can be flexibly implemented in different positions of the pretrained model with competitive unlearning performance achieved. Besides, it also implies that the feature covariance matrices in earlier layers contain sufficient information to achieve MU. Moreover, we provide in Table S4 the corresponding feature dimension d , subspace dimension s and the optimization steps when applying LOFT after different layer modules, which is in relation to the sensitivity analysis results of the right panel in Fig.3. It indicates the additional computation overhead when applying LOFT to earlier layer modules.

Table S4. Hyper-parameters in different positions for LOFT.

position	d	s	steps
layer1	4,096	500	500
layer2	2,048	350	200
layer3	1,024	9	200
layer4	512	9	50

¹https://docs.pytorch.org/vision/main/_modules/torchvision/models/resnet.html#resnet18

Table S5. Training hyper-parameters of different MU methods under extreme unlearning with Swin-T on Tiny-ImageNet.

method	\mathcal{D}_{rm}	\mathcal{D}_{fg}	hyper-parameters
pretrained	✓	✓	20 epochs, lr = 10^{-4} , cosine scheduler
retrained	✓	✗	20 epochs, lr = 10^{-4} , cosine scheduler
FT	✓	✗	10 epochs, lr = 10^{-4} , cosine scheduler
GA	✗	✓	constant scheduler
RL	✗	✓	5 epochs, lr = 5×10^{-7} , cosine scheduler
RL	✓	✓	10 epochs, lr = 2×10^{-5} , cosine scheduler
SalUn	✗	✓	5 epochs, lr = 5×10^{-7} , cosine scheduler, saliency sparsity 50%
SalUn	✓	✓	10 epochs, cosine scheduler, saliency sparsity 50%
BT	✗	✓	2 epochs, lr = 10^{-6} , cosine scheduler, temperature scalar = 1.0
L2UL	✗	✓	lr = 2×10^{-4} , constant scheduler, regularization coefficient = 1.0
COUN+RL	✗	✓	5 epochs, lr = 10^{-4} , cosine scheduler
DELETE	✗	✓	10 epochs, lr = 2×10^{-4} , cosine scheduler
LOFT	only $\Sigma_{\text{rm}}^{\text{pre}}$	only $\Sigma_{\text{fg}}^{\text{pre}}$	50 steps, s = 18, lr = 1, constant scheduler

Table S6. Comparison on performance under extreme unlearning with Swin-T on Tiny-ImageNet.

method	\mathcal{D}_{rm}	\mathcal{D}_{fg}	$\text{Acc}_{\text{rm}}^{\text{tr}}$	$\text{Acc}_{\text{fg}}^{\text{tr}}$	$\text{Acc}_{\text{rm}}^{\text{te}}$	$\text{Acc}_{\text{fg}}^{\text{te}}$	MIA	Avg.G.↓	RTE ↓	# param. (%)
pretrained	✓	✓	99.64 \pm 0.02	99.63 \pm 0.00	75.43 \pm 2.61	74.45 \pm 0.29	95.34 \pm 0.43	-	882.05	27,673,154 (100%)
retrained	✓	✗	99.97 \pm 0.01 (0.00)	0.00 \pm 0.00 (0.00)	90.57 \pm 0.75 (0.00)	0.00 \pm 0.00 (0.00)	0.00 \pm 0.00 (0.00)	0.00	95.17	27,673,154 (100%)
GA	✗	✓	14.26 \pm 6.00 (85.71)	9.61 \pm 4.36 (9.61)	12.20 \pm 4.61 (78.37)	8.10 \pm 3.46 (8.10)	11.41 \pm 5.19 (11.41)	38.64	178.07	27,673,154 (100%)
FT	✓	✗	100.00 \pm 0.01 (0.03)	69.98 \pm 1.24 (69.98)	91.13 \pm 0.86 (0.56)	49.98 \pm 1.03 (49.98)	38.82 \pm 0.58 (38.82)	31.88	47.42	27,673,154 (100%)
RL	✗	✓	26.98 \pm 3.11 (72.99)	16.33 \pm 2.69 (16.33)	23.43 \pm 2.05 (67.14)	13.75 \pm 2.35 (13.75)	5.39 \pm 0.75 (5.39)	35.12	195.26	27,673,154 (100%)
RL	✓	✓	98.77 \pm 0.22 (1.20)	20.40 \pm 0.83 (20.40)	90.03 \pm 0.58 (0.54)	15.38 \pm 0.47 (15.38)	1.10 \pm 0.51 (1.10)	7.72	431.45	27,673,154 (100%)
SalUn	✗	✓	27.39 \pm 0.48 (72.58)	17.57 \pm 3.28 (17.57)	23.30 \pm 2.1 (67.27)	15.05 \pm 2.65 (15.05)	12.25 \pm 1.57 (12.25)	36.95	235.23	13,836,577 (50%)
SalUn	✓	✓	98.72 \pm 0.37 (1.25)	13.88 \pm 3.00 (13.88)	87.93 \pm 1.33 (2.64)	11.61 \pm 2.29 (11.61)	2.74 \pm 1.14 (2.14)	6.31	476.78	13,836,577 (50%)
BT	✗	✓	24.77 \pm 1.40 (75.20)	14.66 \pm 1.40 (14.66)	21.30 \pm 1.32 (69.27)	12.57 \pm 1.30 (12.57)	4.09 \pm 0.44 (4.09)	35.16	88.81	27,673,154 (100%)
L2UL	✗	✓	23.90 \pm 7.94 (76.07)	15.00 \pm 3.50 (15.00)	19.10 \pm 3.53 (71.47)	11.91 \pm 2.50 (11.91)	3.66 \pm 1.95 (3.66)	35.63	7361.76	27,673,154 (100%)
COUN+RL	✗	✓	35.77 \pm 3.93 (64.20)	27.33 \pm 0.42 (27.33)	33.10 \pm 3.50 (57.47)	24.07 \pm 0.25 (24.07)	3.28 \pm 3.46 (3.28)	35.27	337.69	27,673,154 (100%)
DELETE	✗	✓	97.37 \pm 0.36 (2.60)	6.95 \pm 0.31 (6.95)	81.07 \pm 1.53 (9.50)	10.96 \pm 0.48 (10.96)	1.16 \pm 0.16 (1.16)	6.23	446.62	27,673,154 (100%)
LOFT	only $\Sigma_{\text{rm}}^{\text{pre}}$	only $\Sigma_{\text{fg}}^{\text{pre}}$	99.63 \pm 0.18 (0.34)	0.03 \pm 0.03 (0.03)	92.17 \pm 0.65 (1.60)	0.02 \pm 0.02 (0.02)	0.08 \pm 0.12 (0.08)	0.42	0.29	13,824 (0.05%)

D. Extreme Unlearning and Continual Unlearning

D.1. Extreme Unlearning

Settings. We conduct evaluations to investigate the robustness of MU methods under an extreme scenario, where a very high ratio (over 90%) of the training samples is required to be removed. This situation may also arise in practice, such as deleting data across a large number of users on one occasion. In this experiment, 180 of 200 classes (90%) in Tiny-ImageNet are randomly selected as \mathcal{D}_{fg} , and experiments are repeated 3 times. We adopt different random seeds, i.e., 0, 1 and 2, to guarantee that the forgetting 180 labels are different in each experiment. All compared methods use the AdamW optimizer (Loshchilov & Hutter, 2019) with weight decay of 0.05 and a batch size of 128. The hyper-parameters are listed in Table S5. In Table S5, the \mathcal{D}_{fg} -based GA and SalUn involving both \mathcal{D}_{rm} and \mathcal{D}_{fg} are highly-sensitive to the choice of the learning rate under this extreme unlearning scenario. To obtain satisfactory results, we use different learning rates for GA and SalUn in each experiment w.r.t. different random seeds. For GA, the hyper-parameters are $\{4 \text{ epochs, lr} = 3 \times 10^{-7}\}$, $\{7 \text{ epochs, lr} = 2 \times 10^{-7}\}$ and $\{3 \text{ epochs, lr} = 4 \times 10^{-7}\}$ w.r.t. random seeds 0, 1 and 2. For SalUn based on \mathcal{D}_{rm} and \mathcal{D}_{fg} , the hyper-parameters are $\{\text{lr} = 2 \times 10^{-4}\}$, $\{\text{lr} = 1.5 \times 10^{-4}\}$ and $\{\text{lr} = 10^{-4}\}$ w.r.t. random seeds 0, 1 and 2. For L2UL, we only generate two adversarial examples per image for efficiency. Our LOFT optimizes \mathbf{U} through the Riemannian Adam optimizer (Kochurov et al., 2020) with the weight decay of 0.05.

Results. Table S6 demonstrates results of extreme unlearning with Swin-T on Tiny-ImageNet. In this extreme unlearning scenario, methods that directly update f_{pre} struggle to maintain good performances on \mathcal{D}_{rm} , as the gradient updates to f_{pre} are dominated by penalizing performance on \mathcal{D}_{fg} with a substantial number of samples. In contrast, our LOFT does not modify f_{pre} and its projection matrix is optimized on the feature covariances w.r.t. \mathcal{D}_{rm} and \mathcal{D}_{fg} , which is less affected by the relative data sizes of \mathcal{D}_{rm} and \mathcal{D}_{fg} . LOFT achieves the best average gap (Avg.G.) of 0.42 with about 0.05% parameters w.r.t. the given model, and takes the shortest running time (RTE) about 0.29 seconds.

Table S7. Comparison results of Swin-T on Tiny-ImageNet under continual unlearning.

method	\mathcal{D}_{rm}	\mathcal{D}_{fg}	\mathcal{D}_{fgp}	$\text{Acc}_{\text{rm}}^{\text{tr}}$	$\text{Acc}_{\text{fg}}^{\text{tr}}$	$\text{Acc}_{\text{fgp}}^{\text{tr}}$	$\text{Acc}_{\text{rm}}^{\text{te}}$	$\text{Acc}_{\text{fg}}^{\text{te}}$	$\text{Acc}_{\text{fgp}}^{\text{te}}$
<i>Round-1</i>									
pretrained	✓	✓	-	99.63	99.90	-	74.49	80.00	-
retrained	✓	✗	-	99.65 (0.00)	0.00 (0.00)	-	75.08 (0.00)	0.00 (0.00)	-
RL	✗	✓	-	97.00 (2.65)	8.50 (8.50)	-	70.87 (4.21)	1.00 (1.00)	-
RL	✓	✓	-	99.93 (0.28)	4.90 (4.90)	-	74.34 (0.74)	2.00 (2.00)	-
BT	✗	✓	-	98.57 (1.08)	21.60 (21.60)	-	72.58 (2.50)	6.00 (6.00)	-
DELETE	✗	✓	-	99.21 (0.44)	8.00 (8.00)	-	73.87 (0.62)	0.00 (0.00)	-
LOFT	$\Sigma_{\text{rm}}^{\text{pre}}$	$\Sigma_{\text{fg}}^{\text{pre}}$	-	96.86 (2.77)	4.20 (4.20)	-	72.65 (2.43)	0.00 (0.00)	-
<i>Round-2</i>									
pretrained	✓	✓	✓	99.63	99.60	99.90	74.55	69.00	80.00
retrained	✓	✗	✗	99.69 (0.00)	0.00 (0.00)	0.00 (0.00)	75.57 (0.00)	0.00 (0.00)	0.00 (0.00)
RL	✗	✓	✗	80.30 (19.39)	6.30 (6.30)	1.00 (1.00)	59.68 (15.89)	2.00 (2.00)	0.00 (0.00)
RL	✓	✓	✗	99.98 (0.29)	6.30 (6.30)	1.00 (1.00)	74.37 (1.20)	1.00 (1.00)	0.00 (0.00)
BT	✗	✓	✗	91.42 (8.21)	20.30 (20.30)	6.60 (6.60)	67.07 (8.50)	8.00 (8.00)	3.00 (3.00)
DELETE	✗	✓	✗	98.33 (1.30)	10.60 (10.60)	3.90 (3.90)	72.40 (3.17)	5.00 (5.00)	0.00 (0.00)
LOFT	$\Sigma_{\text{rm}}^{\text{pre}}$	$\Sigma_{\text{fg}}^{\text{pre}}$	$\Sigma_{\text{fgp}}^{\text{pre}}$	95.77 (3.92)	7.50 (7.50)	0.50 (0.50)	72.01 (3.56)	4.00 (4.00)	1.00 (1.00)
<i>Round-3</i>									
pretrained	✓	✓	✓	99.62	99.60	99.75	74.53	69.00	74.50
retrained	✓	✗	✗	99.66 (0.00)	0.00 (0.00)	0.00 (0.00)	73.06 (0.00)	0.00 (0.00)	0.00 (0.00)
RL	✗	✓	✗	45.16 (54.50)	0.70 (0.70)	0.30 (0.30)	36.27 (36.79)	0.00 (0.00)	0.50 (0.50)
RL	✓	✓	✗	99.98 (0.32)	7.70 (7.70)	0.30 (0.30)	73.79 (0.73)	2.00 (2.00)	0.00 (0.00)
BT	✗	✓	✗	72.06 (27.60)	6.40 (6.40)	4.45 (4.45)	54.42 (18.64)	1.00 (1.00)	2.50 (2.50)
DELETE	✗	✓	✗	96.27 (3.39)	5.10 (5.10)	3.85 (3.85)	70.05 (3.01)	3.00 (3.00)	1.50 (1.50)
LOFT	$\Sigma_{\text{rm}}^{\text{pre}}$	$\Sigma_{\text{fg}}^{\text{pre}}$	$\Sigma_{\text{fgp}}^{\text{pre}}$	96.39 (3.27)	1.70 (1.70)	0.35 (0.35)	72.80 (0.26)	0.00 (0.00)	0.50 (0.50)
<i>Round-4</i>									
pretrained	✓	✓	✓	99.63	99.30	99.80	74.54	73.00	75.33
retrained	✓	✗	✗	99.67 (0.00)	0.00 (0.00)	0.00 (0.00)	75.72 (0.00)	0.00 (0.00)	0.00 (0.00)
RL	✗	✓	✗	10.96 (88.71)	0.30 (0.30)	0.00 (0.00)	9.97 (65.75)	1.00 (1.00)	0.00 (0.00)
RL	✓	✓	✗	99.98 (0.31)	17.60 (17.60)	1.07 (1.07)	73.43 (2.29)	9.00 (9.00)	0.00 (0.00)
BT	✗	✓	✗	47.28 (52.39)	3.00 (3.00)	1.63 (1.63)	37.69 (38.03)	1.00 (1.00)	0.67 (0.67)
DELETE	✗	✓	✗	93.07 (6.60)	3.80 (3.80)	2.43 (2.43)	67.91 (7.81)	3.00 (3.00)	1.33 (1.33)
LOFT	$\Sigma_{\text{rm}}^{\text{pre}}$	$\Sigma_{\text{fg}}^{\text{pre}}$	$\Sigma_{\text{fgp}}^{\text{pre}}$	96.48 (3.19)	5.50 (5.50)	0.07 (0.07)	72.50 (3.22)	3.00 (3.00)	0.00 (0.00)

D.2. Continual Unlearning

Settings. We provide evaluations for different MU methods under a practical scenario where multiple unlearning requests are in a continual order. To be specific, we consider a 4-round continual unlearning. In each round, 2 classes (1%) are randomly selected as the forgetting data \mathcal{D}_{fg} , and the forgetting labels at each round are {18,170}, {80,49}, {117,51}, and {16,118}, respectively. We introduce two new metrics $\text{Acc}_{\text{fgp}}^{\text{tr}}$ and $\text{Acc}_{\text{fgp}}^{\text{te}}$, i.e., accuracy on the forgetting data in previous rounds \mathcal{D}_{fgp} , to evaluate whether the model indeed forget data from early unlearning requests. Results of continual unlearning are shown in Table S7 including multiple mainstream MU methods.

In this continual unlearning, our LOFT optimizes to guarantee the unlearning performance on forgetting data from previous rounds \mathcal{D}_{fgp} , where we introduce an additional loss J_{fgp} to the objective of $J(\mathbf{U})$ in (2) for achieving the task of continual unlearning as follows:

$$\min_{\mathbf{U} \in \text{St}(d,s)} \underbrace{\left(\frac{\text{Tr}(\mathbf{U}^\top \Sigma_{\text{fgp}}^{\text{pre}} \mathbf{U})}{\text{Tr}(\Sigma_{\text{fgp}}^{\text{pre}})} \right)^2}_{J_{\text{fgp}}} + \underbrace{\left(\frac{\text{Tr}(\mathbf{U}^\top \Sigma_{\text{fg}}^{\text{pre}} \mathbf{U})}{\text{Tr}(\Sigma_{\text{fg}}^{\text{pre}})} \right)^2}_{J_{\text{fg}}} + \underbrace{\left(\frac{\text{Tr}(\Sigma_{\text{rm}}^{\text{pre}} - \mathbf{U} \mathbf{U}^\top \Sigma_{\text{rm}}^{\text{pre}} \mathbf{U} \mathbf{U}^\top)}{\text{Tr}(\Sigma_{\text{rm}}^{\text{pre}})} \right)^2}_{J_{\text{rm}}}. \quad (13)$$

J_{fgp} takes a similar form as J_{fg} and measures the projected variance of the covariance matrix $\Sigma_{\text{fgp}}^{\text{pre}}$ w.r.t. \mathcal{D}_{fgp} captured within the subspace spanned by \mathbf{U} . Hence, minimizing J_{fgp} achieves unlearning on \mathcal{D}_{fgp} . Note that J_{fgp} can be efficiently implemented without additional computation, since $\Sigma_{\text{fgp}}^{\text{pre}}$ has been accessed in previous rounds.

Results. During the multiple rounds of unlearning, other MU methods constantly modify the parameters of the pretrained model f_{pre} and directly affect the learning ability of f_{pre} . As a result, in Table S7, these methods show significant accuracy drops on the remaining data \mathcal{D}_{rm} and even slight accuracy increases on the forgetting data \mathcal{D}_{fgp} in previous rounds, after

Table S8. Training hyper-parameters of different MU methods w.r.t. Table S9 with ResNet50 on VGGFace2.

method	\mathcal{D}_{rm}	\mathcal{D}_{fg}	hyper-parameters
pretrained	✓	✓	200 epochs, lr = 10^{-1} , cosine scheduler
retrained	✓	✗	200 epochs, lr = 10^{-1} , cosine scheduler
FT	✓	✗	10 epochs, lr = 5×10^{-2} , cosine scheduler
GA	✗	✓	5 epochs, lr = 5×10^{-4} , constant scheduler
RL	✗	✓	10 epochs, lr = 5×10^{-4} , cosine scheduler
RL	✓	✓	10 epochs, lr = 5×10^{-2} , cosine scheduler
SalUn	✗	✓	10 epochs, lr = 10^{-4} , cosine scheduler, saliency sparsity 50%
SalUn	✓	✓	10 epochs, lr = 5×10^{-2} , cosine scheduler, saliency sparsity 50%
BT	✗	✓	15 epochs, lr = 5×10^{-4} , cosine scheduler, temperature scalar = 1.0
L2UL	✗	✓	lr = 1×10^{-4} , constant scheduler, regularization coefficient = 1.0
DELETE	✗	✓	10 epochs, lr = 5×10^{-4} , cosine scheduler
LOFT	only $\Sigma_{\text{rm}}^{\text{pre}}$	only $\Sigma_{\text{fg}}^{\text{pre}}$	50 steps, s = 21, lr = 1, constant scheduler

Table S9. Comparison results of ResNet50 on VGGFace2, forgetting one of 200 identities.

method	\mathcal{D}_{rm}	\mathcal{D}_{fg}	$\text{Acc}_{\text{rm}}^{\text{tr}}$	$\text{Acc}_{\text{fg}}^{\text{tr}}$	$\text{Acc}_{\text{rm}}^{\text{te}}$	$\text{Acc}_{\text{fg}}^{\text{te}}$	MIA	Avg.G.↓	RTE ↓	# param. (%)
pretrained	✓	✓	100.00	100.00	98.15	99.49	100.00	-	5970.95	25,557,032 (100%)
retrained	✓	✗	100.00 (0.00)	0.00 (0.00)	98.21 (0.00)	0.00 (0.00)	0.00 (0.00)	0.00	5870.35	25,557,032 (100%)
GA	✗	✓	91.91 (8.09)	0.00 (0.00)	86.34 (11.87)	0.00 (0.00)	0.00 (0.00)	4.00	3.35	25,557,032 (100%)
FT	✓	✗	99.84 (0.16)	0.00 (0.00)	96.22 (1.99)	0.00 (0.00)	0.00 (0.00)	0.43	294.62	25,557,032 (100%)
RL	✗	✓	99.64 (0.36)	11.25 (11.25)	95.27 (2.94)	13.20 (13.20)	0.00 (0.00)	5.55	5.59	25,557,032 (100%)
RL	✓	✓	99.11 (0.89)	0.00 (0.00)	94.66 (3.55)	0.00 (0.00)	0.00 (0.00)	0.89	303.81	25,557,032 (100%)
SalUn	✗	✓	99.68 (0.32)	5.50 (5.50)	95.59 (2.62)	5.08 (5.08)	0.00 (0.00)	2.70	9.99	12,778,516 (50%)
SalUn	✓	✓	99.96 (0.04)	0.00 (0.00)	97.00 (1.21)	0.00 (0.00)	0.00 (0.00)	0.25	312.71	12,778,516 (50%)
BT	✗	✓	99.39 (0.61)	5.00 (5.00)	94.97 (3.24)	4.06 (4.06)	0.00 (0.00)	2.58	8.24	25,557,032 (100%)
L2UL	✗	✓	98.09 (1.91)	2.75 (2.75)	92.88 (5.33)	3.55 (3.55)	0.00 (0.00)	2.71	176.69	25,557,032 (100%)
DELETE	✗	✓	99.50 (0.50)	5.50 (5.50)	95.15 (3.06)	5.58 (5.58)	0.00 (0.00)	2.93	5.82	25,557,032 (100%)
LOFT	only $\Sigma_{\text{rm}}^{\text{pre}}$	only $\Sigma_{\text{fg}}^{\text{pre}}$	97.20 (2.80)	0.00 (0.00)	94.22 (3.99)	0.51 (0.51)	0.00 (0.00)	1.46	0.45	43,008 (0.17%)

4 rounds of unlearning. In contrast, our LOFT does not update parameters of the pretrained f_{pre} , and well preserves the learning ability of f_{pre} . By only optimizing the projection matrix \mathbf{U} given $\Sigma_{\text{rm}}^{\text{pre}}$, $\Sigma_{\text{fg}}^{\text{pre}}$ and $\Sigma_{\text{fgp}}^{\text{pre}}$, the learned subspace of LOFT successfully maintains the accuracy on \mathcal{D}_{rm} and reduces the accuracy on \mathcal{D}_{fg} and \mathcal{D}_{fgp} .

E. Applications: Face Recognition and Emotion Recognition

Both identities and emotions are key facial attributes closely related to user privacy. Exploring the unlearning of such information can benefit privacy protection. Thereby we investigate MU for this two real-world applications of face recognition and emotion recognition.

E.1. Face Recognition with Machine Unlearning

Settings. Experiments are conducted on a prevalent face identity recognition dataset VGGFace2 (Cao et al., 2018), including approximately 3.31 million images collected from 9,131 identities. Particularly, we adopt its publicly-available version², where all face images are aligned and cropped to $112 \times 112 \times 3$. Our experiments utilize a filtered set of 200 identities, each with over 500 images. Then, we randomly select 400 images for each identity, forming a training set containing 80,000 images, and the rest is adopted as the test set. One of the 200 identities (0.5%) is randomly selected as the forgetting data \mathcal{D}_{fg} , which is a challenging setting for class-centric unlearning. The adopted neural network model is ResNet50 (He et al., 2016). All the compared methods use the SGD optimizer (Bottou, 2012) with a weight decay of 5×10^{-4} , the momentum of 0.9, and a batch size of 128. More training details are in Table S8 with comparison results in Table S9.

Results. This unlearning setting, i.e., forgetting one of the 200 identities, implies a substantial size of \mathcal{D}_{rm} . Therefore, MU methods involving \mathcal{D}_{rm} can easily achieve the ideal performance of the exact unlearning model of f_{exact} , as illustrated

²<https://www.kaggle.com/datasets/yakhyokhuja/vggface2-112x112>

Table S10. Training hyper-parameters of different MU methods w.r.t. Table S11 with ResNet18 on RAF-DB.

method	\mathcal{D}_{rm}	\mathcal{D}_{fg}	hyper-parameters
pretrained	✓	✓	200 epochs, lr = 10^{-1} , cosine scheduler
retrained	✓	✗	200 epochs, lr = 10^{-1} , cosine scheduler
FT	✓	✗	10 epochs, lr = 5×10^{-2} , cosine scheduler
GA	✗	✓	10 epochs, lr = 5×10^{-4} , constant scheduler
RL	✗	✓	20 epochs, lr = 5×10^{-4} , cosine scheduler
RL	✓	✓	10 epochs, lr = 5×10^{-2} , cosine scheduler
SalUn	✗	✓	20 epochs, lr = 10^{-4} , cosine scheduler, saliency sparsity 50%
SalUn	✓	✓	10 epochs, lr = 5×10^{-2} , cosine scheduler, saliency sparsity 50%
BT	✗	✓	15 epochs, lr = 5×10^{-4} , cosine scheduler, temperature scalar = 1.0
L2UL	✗	✓	lr = 2×10^{-4} , constant scheduler, regularization coefficient = 1.0
DELETE	✗	✓	20 epochs, lr = 2×10^{-4} , cosine scheduler
LOFT	only $\Sigma_{\text{rm}}^{\text{pre}}$	only $\Sigma_{\text{fg}}^{\text{pre}}$	50 steps, $s = 6$, lr = 1, constant scheduler

Table S11. Comparison results of ResNet18 on RAF-DB.

method	\mathcal{D}_{rm}	\mathcal{D}_{fg}	$\text{Acc}_{\text{rm}}^{\text{tr}}$	$\text{Acc}_{\text{fg}}^{\text{tr}}$	$\text{Acc}_{\text{rm}}^{\text{te}}$	$\text{Acc}_{\text{fg}}^{\text{te}}$	MIA	Avg.G.
pretrained	✓	✓	100.00	100.00	85.10	56.76	100.00	-
retrained	✓	✗	100.00 (0.00)	0.00 (0.00)	84.90 (0.00)	0.00 (0.00)	0.00 (0.00)	0.00
GA	✗	✓	91.38 (8.62)	0.36 (0.36)	76.75 (8.15)	0.00 (0.00)	0.36 (0.36)	3.50
FT	✓	✗	99.97 (0.03)	0.00 (0.00)	83.97 (0.03)	0.00 (0.00)	0.00 (0.00)	0.01
RL	✗	✓	98.96 (1.04)	15.66 (15.66)	79.93 (4.97)	5.41 (5.41)	0.00 (0.00)	5.42
RL	✓	✓	99.92 (0.08)	0.00 (0.00)	84.10 (0.80)	0.00 (0.00)	0.00 (0.00)	0.18
SalUn	✗	✓	99.83 (0.17)	12.46 (12.46)	82.53 (2.37)	2.70 (2.70)	0.36 (0.36)	3.61
SalUn	✓	✓	99.98 (0.02)	0.00 (0.00)	84.57 (0.33)	0.00 (0.00)	0.00 (0.00)	0.07
BT	✗	✓	99.83 (0.17)	10.68 (10.68)	82.63 (2.27)	2.70 (2.70)	1.07 (1.07)	3.38
L2UL	✗	✓	99.99 (0.01)	10.68 (10.68)	84.03 (0.87)	1.35 (1.35)	0.00 (0.00)	2.58
DELETE	✗	✓	99.72 (0.28)	9.25 (9.25)	82.20 (2.70)	2.70 (2.70)	1.42 (1.42)	3.27
LOFT	only $\Sigma_{\text{rm}}^{\text{pre}}$	only $\Sigma_{\text{fg}}^{\text{pre}}$	100.00 (0.00)	0.00 (0.00)	84.90 (0.00)	0.00 (0.00)	0.00 (0.00)	0.00

by the FT, RL (w/ \mathcal{D}_{rm}), and SalUn (w/ \mathcal{D}_{rm}) in Table S9. In contrast, it is challenging for MU methods by only accessing \mathcal{D}_{fg} under this unlearning setting, as demonstrated by the relatively high accuracy on \mathcal{D}_{fg} of RL (w/o \mathcal{D}_{rm}), SalUn (w/o \mathcal{D}_{rm}), BT, L2UL and DELETE in Table S9. Our LOFT does not visit the original samples and learns to preserve and remove essential patterns from the feature covariance matrices of \mathcal{D}_{rm} and \mathcal{D}_{fg} through low-dimensional projections, managing to simultaneously maintain high accuracy on \mathcal{D}_{rm} and suppress accuracy on \mathcal{D}_{fg} .

E.2. Emotion Recognition with Machine Unlearning

Settings. Experiments are conducted on a popular emotion recognition dataset RAF-DB (Li et al., 2017), RAF-DB contains 12,271 and 3,068 training and test images with a size of $100 \times 100 \times 3$, respectively, within 7 different emotions: “surprise”, “fear”, “disgust”, “happiness”, “sadness”, “anger” and “neutral”. In the experiments, one emotion is randomly selected as the forgetting data \mathcal{D}_{fg} (“fear”). The adopted model is ResNet18 (He et al., 2016). All the compared methods use the SGD optimizer (Bottou, 2012) with a weight decay of 5×10^{-4} , the momentum of 0.9, and a batch size of 128. More training details are listed in Table S10. The comparison results among different MU methods are shown in Table S11.

Results. As illustrated in Table S11, when forgetting the “fear” emotion from the total 7 emotions, LOFT shows the best approximation performance towards that of the retrained model f_{exact} . Other MU methods either heavily rely on the remaining data \mathcal{D}_{rm} (RL and SalUn), or show unsatisfactory results on \mathcal{D}_{fg} (BT, L2UL and DELETE). LOFT explores the low-dimensional subspace in which the features of \mathcal{D}_{fg} and \mathcal{D}_{rm} can be well distinguished through its reconstruction performances, achieving distinctively better unlearning performances.

F. Low-Dimensional Feature Subspaces for MU in Generation Tasks

In this section, we provide a preliminary exploration of using low-dimensional feature subspaces for machine unlearning in generation tasks. As our LOFT does not update the parameters of the pretrained model f_{pre} , LOFT is not directly applicable to models in generation tasks. Meanwhile, there are distinctively different generation models in different tasks. For example, in image generation, the convolution network in DDPM (Ho et al., 2020) and LDM (Rombach et al., 2022) significantly differs from the vision transformer in DiT (Peebles & Xie, 2023), while the transformer itself functions differently between image generation and language-related generation tasks (Liu et al., 2025). Another challenge is that generative models are particularly sensitive to internal changes in their feature representations. For instance, even subtle alterations in the intermediate layers of a DDPM can lead to artifacts or meaningless pixels in the generated images. Therefore, crafting an appropriate low-dimensional feature subspace must be carefully tailored to the specific generative model and the particular unlearning scenario. This direction, to the best of our knowledge, still remains underexplored. In the following, we present promising unlearning results from LOFT applied to a *machine translation* task. This initial success suggests the potential of our feature subspace perspective for MU in generative tasks, and we hope it will advocate further research in this area.

Settings. We evaluate LOFT on a machine translation task with an unlearning target as *forcing the model to forget the ability of translating a specific language*. This natural language processing task is not a classification one and the subspace shall not be tightly coupled with class-specific features. The experiment is conducted on the WMT-19 dataset³ and a modern large model named m2m100_1.2B⁴. The pretrained m2m100_1.2B model is fine-tuned in a parameter-efficient way (i.e., LoRA) on two language pairs from WMT-19: translating Czech into English and translating Lithuanian into English. This fine-tuned m2m100_1.2B model is adopted as the initial startpoint to be unlearned, and the to-be-unlearned language is Lithuanian.

Implementation. With this modern large model of m2m100_1.2B, we apply LOFT to the *hidden states* from the output of the encoder of m2m100_1.2B. Specifically, the token-level hidden states get weighted averaged by the self-attention from the encoder and lead to weighted averaged 1024-dimensional features, where 1024 is the hidden dimension of m2m100_1.2B. In this way, we avoid the massive tokens and extremely large vocabulary size and focus on the attention-based weighted average features to apply LOFT. Then, two feature covariance matrices are calculated w.r.t. Czech and Lithuanian inputs, and the optimization objective of LOFT in (2) is conducted to learn a projection matrix. In inference, the projector is employed at the token-level hidden states to proceed the propagation, similar as the way in Sec.5.3.

Results. Our results are presented in the following Table S12. We evaluate translation quality using the BLEU score (Papineni et al., 2002) on the WMT-19 validation set for Czech-to-English (cs→en) and Lithuanian-to-English (lt→en) directions. The forgetting data (fg) and remaining (rm) data correspond to the lt→en and cs→en pairs, respectively. Here, fully-trained denotes m2m100_1.2B fine-tuned on both language pairs, while retrained refers to m2m100_1.2B trained exclusively on the remaining (cs→en) data without seeing (lt→en) inputs. Blue numbers in parentheses denote the BLEU score gap relative to the retrained method (lower is better). After unlearning, our LOFT achieves performance on the forgetting language pair (lt→en) that is very close to the retrained model, implying successful forgetting of the Lithuanian-to-English translation capability. Meanwhile, LOFT maintains good performance on the remaining Czech-to-English direction, demonstrating effective knowledge preservation. As an exemplary trial on large language models, this experiment validates LOFT’s potential for extension to non-classification tasks and its scalability to modern large models.

Table S12. Results of LOFT on machine translation with a modern large model of m2m100_1.2B.

method	cs→en (rm)	lt→en (fg)
fully-trained	27.63	17.54
retrained	26.19	12.31
GA	23.51 (2.68)	15.79 (3.48)
LOFT	22.88 (3.31)	13.04 (0.73)

³<https://huggingface.co/datasets/wmt/wmt19>

⁴https://huggingface.co/facebook/m2m100_1.2B

G. Further Discussions on Separability, Scalability and Privacy Protection

Separability. LOFT is built on the separability between \mathcal{D}_{fg} and \mathcal{D}_{rm} in low-dimensional feature subspaces in the general unlearning context. We highlight that the discussed separability is different from the separability in supervised classification. Given f_{pre} pretrained on the full data, its learned features of \mathcal{D}_{fg} and \mathcal{D}_{rm} are separable according to the supervised classification labels. However, considering the separability between \mathcal{D}_{fg} and \mathcal{D}_{rm} in low-dimensional subspaces without the labels, our reconstruction analysis in Sec.3 validates that their features from f_{pre} are indistinguishable as both \mathcal{D}_{fg} and \mathcal{D}_{rm} have been involved into training, while the retrained model f_{exact} demonstrates separability. This motivates our LOFT by investigating whether it is possible to formulate linear transformations (subspace learning) to features from f_{pre} , such that the knowledge of forgetting features can be diminished and that of remaining features is meanwhile well kept. Apart from approaching the outputs or parameters of the exact retrained model, it would be an interesting and promising direction to formulate an unlearning model that pertains similar properties in feature (sub)spaces, which we hope could bring new insights and opportunities to approximate machine unlearning.

Scalability. The two covariance matrices in LOFT only require one-shot fetching to features of raw data, which is achieved within one network forward pass. We highlight that this one-shot feature fetching is a key advantage of LOFT for its scalability. Mainstream unlearning methods face significant scalability bottlenecks: they either (i) require *repeated forward-backward* passes on full data with gradients calculations, which is prohibitively expensive for large-scale data, or (ii) rely solely on the forgetting data for efficiency, but leading to limited performance due to the absence of the remaining data information. In contrast, LOFT processes the training data in a *single forward* pass, eliminating the need for backward propagation. We think such computational complexity of LOFT is acceptable for deep learning in practice and makes LOFT particularly suitable for large-scale data scenarios. For example, the ImageNet-1K dataset includes over 1.28M training images. Existing methods that calculates gradients on both forgetting and remaining data with multiple epochs face nearly prohibitive calculations on ImageNet-1K, while LOFT can be efficiently and effectively executed by iterating the ImageNet-1K training dataset only once. Therefore, LOFT strikes a favorable balance and achieves effective unlearning by leveraging the forgetting and remaining feature covariance matrices through a single, computationally-manageable forward pass, thereby offering remarkable scalability in practical applications.

Privacy protection against white-box attacks. One may argue that the privacy protection of LOFT can be easily broken under *white-box* attacks, where attackers are aware of the complete information of LOFT, including (i) the backbone, (ii) our plug-in module, and (iii) the position of our plug-in module. In this case, a simple erasure on the plug-in projection module of LOFT exposes the vanilla pretrained model. We discuss this potential white-box attack from the following aspects.

- In principle, any unlearning method would be vulnerable to privacy leakage if white-box attacks happen, as white-box attackers can access model parameters and their gradients and hold full knowledge of the internal unlearning mechanism. White-box attacks are extremely risky scenarios with privacy leakage and are somehow impractical.
- The plug-in module of LOFT can be absorbed into the network parameters with only single model released. The key of LOFT lies in learning projectors for features, which can be conducted at different layers of the pretrained network. This learned projection matrix \mathbf{U} can be seamlessly integrated into the layer parameters of the network. For example, when applied to the penultimate layer (default setting), our projectors $\mathbf{U}\mathbf{U}^\top$ can be directly absorbed into the weight \mathbf{W} of the last linear layer, i.e., $\mathbf{W} \leftarrow \mathbf{W}\mathbf{U}\mathbf{U}^\top$. Thus, in practice, this allows us to release a single model without maintaining a separate projection module $\mathbf{U}\mathbf{U}^\top$. Further note that this absorption is similarly applicable across different layers for LOFT with a single updated model released. By such implementation, some simple tests, such as a module-level erasure test, are not that simple and straightforward, as one has to be able to decouple different layers of the released single model and then to test through them to figure out the implementation position of the module for next steps.
- We would like to highlight another advantage of LOFT in privacy protection particularly during the unlearning stage. Existing methods iteratively visit the raw data and compute the parameter gradients of the whole network, hence the attackers could have more chances to access such process to steal raw data or get/estimate gradients, posing privacy leakage during unlearning. Our LOFT does not require iterative accesses to the raw data nor model parameters/gradients and thus has less exposure to model information, which could be to some extent a way to mitigate privacy leakage in this sense. This property should not be overlooked.